Abstract—The surf silverside (*Notocheirus hubbsi*) is a rare and poorly known species within Notocheiridae. However, 2 collections of larval and juvenile specimens in Chile provided an opportunity to study unknown aspects of its morphological development and early life history. This study describes the ossification process and provides a detailed osteological description of the juvenile stage which is compared with adult descriptions available from the literature. Features are described in detail for comparative purposes with members of other atheriniform species, especially of the genus *Iso*. A single epural is present in larval stages of *Notocheirus* but is absent in juvenile and adult stages, hence, *Iso* and *Notocheirus* share the presence of a single epural, whereas other atheriniforms have 2 epurals. The pattern of *Notocheirus* supraorbital sensory canal pores is shared with that of Atherinopsinae. Our expectation is that similarities such as these may be tested as homologies, aiding in the resolution of competing hypotheses of relationships and family-level classification. Spinoid scales and odontodes associated with dermal bones of the head are unique for *Notocheirus*, however they not always present in juvenile and adult specimens. The crown of odontodes on the snout are not associated to any bones and appear to be unique for *Notocheirus* as well.

Osteological development of the surf silverside *(Notocheirus hubbsi)* (Teleostei: Atheriniformes: Notocheiridae)

Brian S. Dyer (contact author)[1]
Francisca Zavala-Muñoz[2]
Valentina Bernal-Durán[2,3]
Mauricio F. Landaeta[2,4,5]

Email address for contact author: briansdyer@gmail.com

[1] Centro de Estudios Generales
Universidad de los Andes
Avenida Monseñor Álvaro del Portillo 12.455
Las Condes, Santiago, Chile

[2] Laboratorio de Ictiología e Interacciones Biofísicas (LABITI)
Instituto de Biología, Facultad de Ciencias
Universidad de Valparaíso
Avenida Gran Bretaña 1111
Playa Ancha, Valparaíso, Chile

[3] Programa de Doctorado en Ciencias mención Ecología y Biología Evolutiva
Universidad de Chile
Las Palmeras 3425
Ñuñoa, Santiago, Chile

[4] Centro de Observación y Análisis del Océano Costero (COSTA-R)
Universidad de Valparaíso
Montaña 885
Viña del Mar, Valparaíso, Chile

[5] Millennium Nucleus for Ecology and Conservation of Temperate Mesophotic Reef Ecosystems (NUTME)
Osvaldo Marín 1672
Las Cruces, Valparaíso, Chile

Introduction

Atheriniformes include around 388 species of marine, estuarine, and freshwater fishes (Fricke et al., 2024) commonly known as silversides, hardyheads, rainbowfishes, and blue eyes (Nelson et al., 2016). The surf silverside (*Notocheirus hubbsi*) described by Clark (1937) and placed in Atherinidae (commonly known as Old World silversides), is a small species with an unusual morphology among Atheriniformes (Fig. 1), such as absence of the first dorsal fin, a laterally compressed tear-drop body with a ventral abdominal keel, the lack of several bones of the head, highly modified paired girdles and fins, head and body with spinoid scales, and presence of odontodes (dermal denticles of Sire and Allizard [2001]) on dermal bones of the skull. *Notocheirus* and *Iso* share the laterally compressed and tear-drop body shape, which is deepest at the pectoral fins that are positioned high over the body midline, and the modified pectoral and pelvic girdles that form a sharp ventral keel. All these features have been used as evidence of their close relationship, but were also interpreted as adaptations to the high-energy surf environment inhabited by the members of these genera (Saeed et al., 1994). The first phylogenetic systematic studies of Atheriniformes based on morphology (Saeed et al., 1994; Dyer and Chernoff, 1996) supported the traditional view of *Notocheirus* and *Iso* as sister taxa. However, recent genetic-based phylogenies have placed *Notocheirus* in the subfamily Notocheirinae within Atherinopsidae and *Iso* in Isonidae as sister group to Atherinidae (Bloom et al., 2012; Campanella et al., 2015; Betancur-R et al., 2017), rendering the shared similarities questionable (Bloom et al., 2012). Analyzing the ontogeny of these morphological similarities may shed light on whether some of these features are

Figure 1

Photograph of the left side of a juvenile surf silverside (*Notocheirus hubbsi*) (31.20 mm standard length) caught in Mineral de Talca, Coquimbo, Chile on 23 February 2015. Specimen courtesy of Sergio Carrasco, and photograph courtesy of Claudio Quezada-Romegialli.

homologous or convergent functional adaptations to surf environments.

Notocheirus hubbsi is distributed from Coquimbo, Chile (southeastern Pacific Ocean) and Puerto Deseado, Argentina (southwestern Atlantic Ocean), to the southern tip of Tierra del Fuego (Dyer and Chernoff, 1996; Carrasco et al., 2017; Díaz-Astudillo et al., 2019). Most studies regarding this species have provided morphological information for systematic studies (Said, 1983; Saeed et al., 1994; Dyer and Chernoff, 1996; Saeed et al., 2006), but close to nothing is known about its development, biology, or ecology except that it is planktivorous with a low fecundity (Gosztonyi, 1972). Also, the lunar cycle affects the abundance of early life-stages in nearshore habitats (Zavala-Muñoz et al., 2021). Although *N. hubbsi* is extremely rare, a larger number of post larval and juvenile stages have been collected recently (Carrasco et al., 2017; Díaz-Astudillo et al., 2019). Despite the lack of adult specimens to complete the description of the ossification process, most elements of the skeleton are almost completely ossified at the juvenile stage, based on previously published descriptions (Rosen, 1964; Said, 1983; Saeed et al., 1994; Dyer and Chernoff, 1996; Saeed et al., 2006) and data collected by the first author.

In this paper, a detailed description of the developmental osteology in larvae and juveniles of *N. hubbsi* is presented, some of our findings are compared with information of other atheriniforms available in the literature, and homology statements are discussed.

Materials and methods

Light traps were used to collect 19 specimens, from which 16 larvae (7.89–16.21 mm standard length [SL]) were obtained during the mid-austral spring (October–December 2015), and 3 juveniles (30.77–34.62 mm SL) during summer (January 2016, December 2016, February 2017), respectively. The specimens were collected in El Quisco Bay (33°24′S, 71°42′W), central Chile, using light traps (Ecocean, Montpellier, France), installed weekly on a lunar basis (centered in first quarter, full moon, third quarter, and new moon) between Septem-

ber 2015 and February 2016, and between September 2016 and February 2017. Each Ecocean trap consisted of a buoyant water-tight block containing a 12V battery and a 55 W 90 LED light, under which was attached, in a vertical position, a 2-m long conical net with a 2-mm mesh and a narrow funnel in the middle. Three light traps were deployed on the surface over a bottom depth of about 20 m using a moored buoy and at 500 m from shore. The codends were removed at the end of each evening, and the catch were treated with benzocaine (BZ–20, Veterquímica, Santiago, Chile) before preservation in 96% ethanol (Díaz-Astudillo et al., 2019).

Measurements were made to the nearest 0.01 mm using a digital caliper. Six larvae, ranging from 7.89 mm to 16.21 mm SL, and one 31.16-mm-SL juvenile were cleared and double stained following a modified version of Dingerkus and Uhler (1977), and analysed with a Zeiss Stemi SV 11 (Carl Zeiss AG, Oberkochen, Germany). Anatomical nomenclature was adopted from Schultze and Arratia (1989), Dyer and Chernoff (1996), Dyer (1997), Arratia et al. (2001), Arratia (2008), and Bräger and Moritz (2016). Illustrations were made by the second author in Procreate, vers. 5.2.6 (Savage Interactive Pty Ltd., Hobart, Tasmania) based on drawings taken from a Zeiss' camera lucida. The 19 specimens were deposited at the Museo de Historia Natural de Valparaíso, under the codes MHNV 832–840. Comparative materials of adults were: *Notocheirus hubbsi*: CAS 5525 (holotype); Museum Zoology University of Michigan UMMZ 231951; Museo de Zoología Universidad de Concepción, MZUC 18406, 22479; Instituto de Zoología Universidad Austral IZUA-MP 636; *Iso rhothophilus*: UMMZ 217631, 212579; *Dentatherina merceri*: FMNH 99632; and *Atherion elymus*: UMMZ 204128.

Results

Each bone or group of bones are first described as they appear in the juvenile 31.16-mm-SL specimen, followed by the ontogenetic development of the bones as they appear in the size series at hand. All descriptions in the text and the illustrations that accompany them (Figs. 2–11) refer to the juvenile unless otherwise specified.

Neurocranium

Ethmoid region

The ethmoid cartilage is a large and bulbous structure to which all elements of this region are connected (Fig. 2). It projects posteriorly towards the interorbital cartilage between the frontal and the parasphenoid. It is rounded anteriorly (Fig. 3A) with a bulging lateral process that is flattened laterally (Fig. 3, A and B) to which the lacrimal, the tip of the pars autopalatina, and maxilla are connected (Fig. 2). The nasal capsules are fully separated by the ethmoid cartilage which is wider and deeper at the preorbital region (Fig. 3A), where it extends ventro-medially as a single continuous unit under the parasphenoid (Fig. 3, B and C). The ethmoid cartilage extends ventrally to the parasphenoid in larvae 7.89 to 16.21 mm SL, but does not extend below and under it as in the juvenile. The preorbital region of the ethmoid cartilage has a vertically oriented lateral rim articulated with the lacrimal, and a horizontally oriented ventral rim that articulates with the pars autopalatina.

The lateral ethmoid forms the posterior wall of the nasal capsule and the anterior wall of the orbit (Figs. 2 and 3, B and C). This bone is flattened antero-posteriorly at the center and expanded dorsally, laterally, and ventrally. The lateral ethmoid is expanded dorsally but does not reach the nasal bone or the anterior end of the frontal in the juvenile. This bone barely reaches the lateral rim that has a vertically elongated cartilaginous surface articulated with the lacrimal (Fig. 3A). The ventral cartilaginous rim is transversally oriented and articulates with the medial process of the pars autopalatina (Fig. 2). The preorbital ethmoid cartilage is continuous medially with the interorbital cartilage to form the anterior myodome and the medial extension ventral to the parasphenoid (Figs. 2 and 3B). A lateral ethmoid ossification is not observed at 7.89 mm SL but is present as an incipient ossification at 9.77 mm SL, at the center of the preorbital section of the ethmoid cartilage and extended radially in larger larvae in a roughly circular shape, but not fully ossified in the juvenile specimen.

The nasal is a thin dorsally concave bone, which slightly overlaps the antero-medial edge of the frontal (Fig. 3A). It is widest at its middle and the anterior tip is gently curved ventrally around the anterior part of the nasal capsule to join the lacrimal-pars autopalatina-nasal juncture (Fig. 2). The nasal contains the anterior section of the supraorbital sensory canal with 2 membranous pores. It is visible first at 9.77 mm SL, clearly ossified at 13.82 mm SL, and completely ossified by 16.21 mm SL.

A cluster of 10 tooth-like spines of dermal origin, grouped together in a circle resembling a crown of spines (Figs. 2 and 3, A and B), is located dorso-anteriorly of the ethmoid cartilage and is not associated with any bone or underlying scale or cartilage. A vomer and mesethmoid are lacking (Figs. 2 and 3A–C) as is the case for adults.

Orbital region

The frontal (=parietal of Schultze [2008]) is the largest bone of the neurocranium, forming the roof of the orbit and anterior half of the otic region (Fig. 3, A and B). It is roughly triangular in shape and partially ossified along

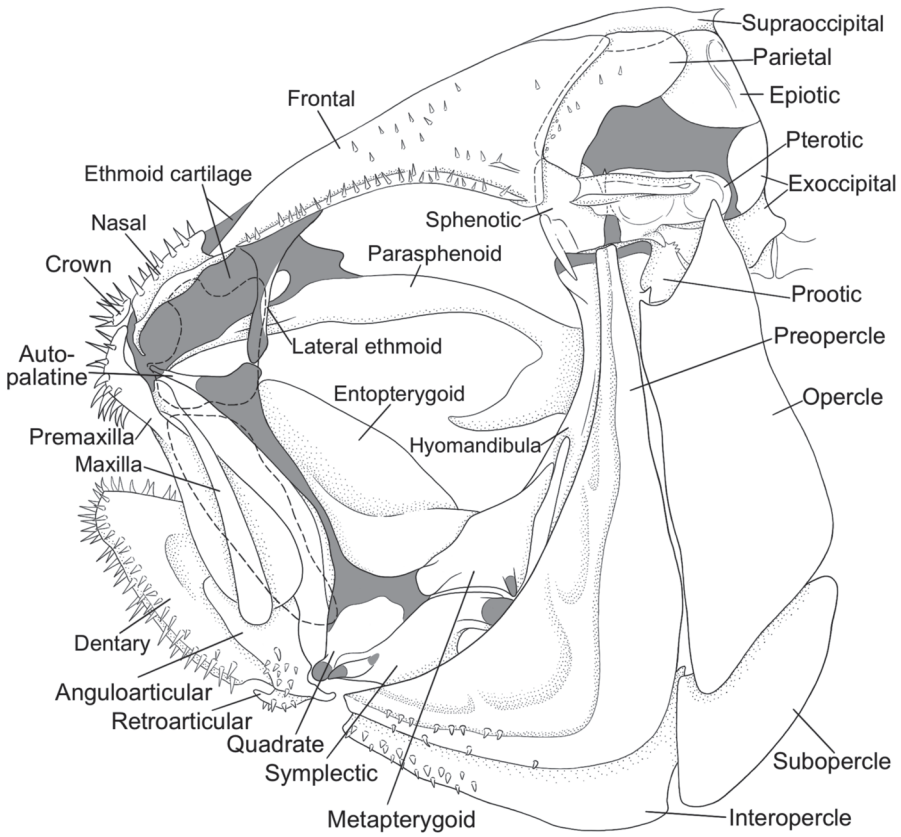

Figure 2

Illustration of the head in lateral view of a surf silverside (*Notocheirus hubbsi*) (31.16 mm standard length) caught in El Quisco Bay, Chile, on 19 January 2016. Dashed lines correspond to the outline of anterior infraorbital bones, extension of sphenotic and parietal under the frontal, and supraoccipital under the parietal.

the lateral and posterior margins at 9.77 mm SL. Anteriorly it articulates with the nasal and ethmoid cartilage, overlapping the posterior end of the nasal capsules. Posteriorly, the frontal is sutured to the supraoccipital, parietal, and sphenotic (Fig. 3A). Medially, the counterparts alternate overlapping each other, except for the anterior one-fifth over the ethmoid cartilage where both separate (Fig. 3A). All sensory canals of the head are open canals with odontodes on the lateral and medial bony ridges (Fig. 3, A and B). The frontal carries the supraorbital sensory canal with pore 3 which opens antero-laterally, and pores 4 and 5 which open postero-medially (Fig. 3A). The sensory canal system continues anteriorly with pore 2 on the nasal bone and continues posteriorly into the otic canal, with pore 6 between both canals (Fig. 3A). Odontodes are also present medially on the frontals in a sparsely uniform pattern, seen only in juvenile and adult specimens (Fig. 3, A and B).

Anteriorly, the parasphenoid is a laminar bone flattened dorso-ventrally and joined to the ventral surface of the ethmoid cartilage, through which it traverses at the preorbital region (Fig. 3, B and C). More posteriorly, it appears as an inverted *T* in cross-section, not contacting the lateral ethmoid (Fig. 3, B and C). Between the lateral ethmoid and the prootic, the parasphenoid shaft is notably arched postero-ventrally as a laterally compressed blade-like process that is widest at the interorbital cartilage (Figs. 2 and 3B). Posterior to the orbit, the parasphenoid extends under the ventral portion of the prootic and the anterior half of the basioccipital, forming the floor of the posterior myodome (Fig. 3, B and C). Ventral to the enlarged anterior opening of the posterior myodome is a dorso-lateral wing (ascending process) on either side sutured to the prootic (Fig. 3, B and C). Ventrally is a curved medial process that extends towards the entopterygoid (Figs. 2 and 3B). The main shaft of the parasphenoid is ossified and relatively straight at 7.89 and 9.77 mm SL, with incomplete ossification at the anterior end ventral to the ethmoid cartilage, at the posterior end ventral to the basioccipital,

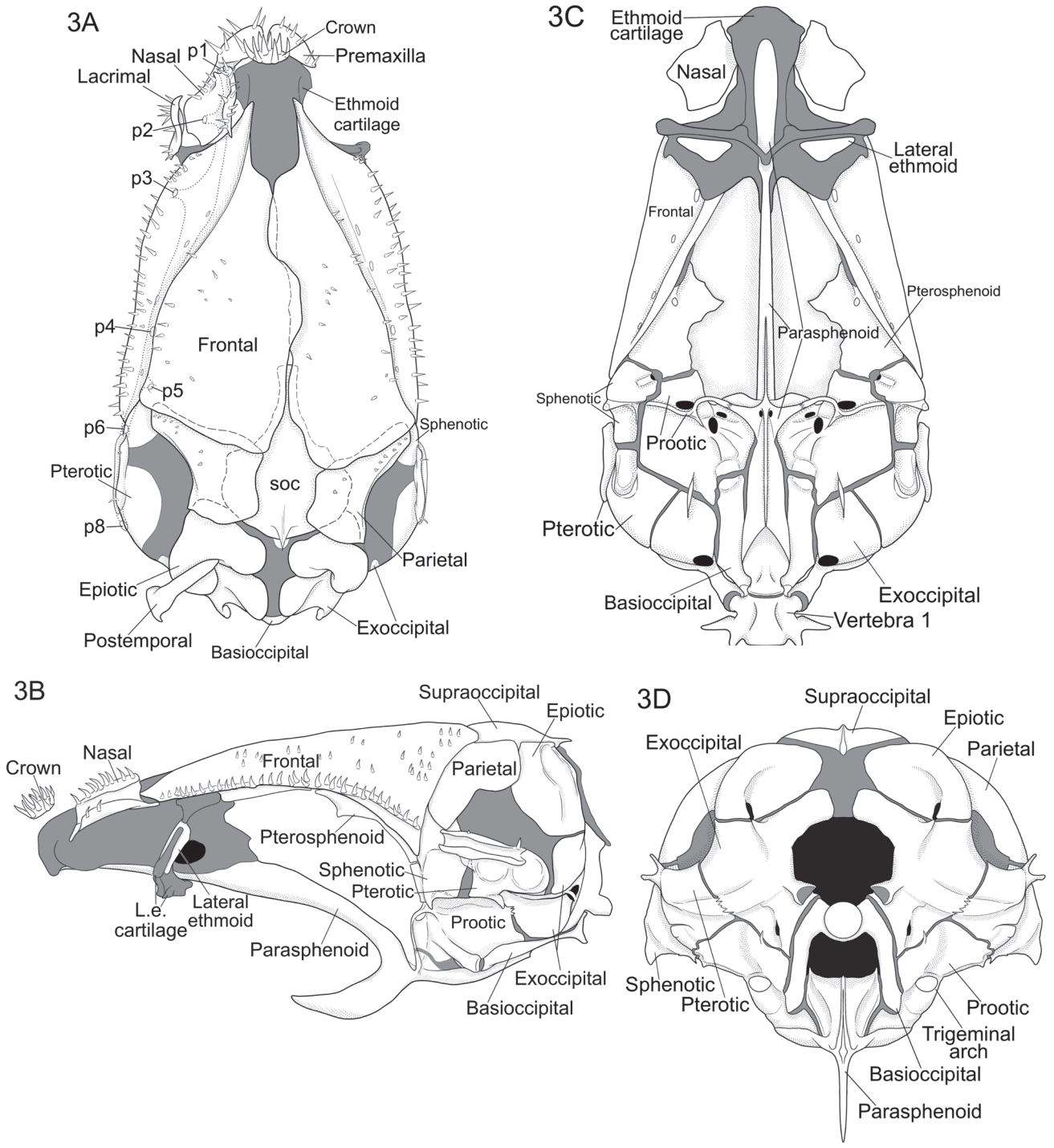

Figure 3

Illustrations of the neurocranium from different viewpoints of a surf silverside (*Notocheirus hubbsi*) (31.16 mm standard length) caught in El Quisco Bay, Chile, on 19 January 2016; soc=supraoccipital; L.e.=Lateral ethmoid. (**A**) Dorsal view. Dotted lines on the left side show the supraorbital sensory canal and pores (p1–p8). Dashed lines are extensions of bones underlying neighboring bones. (**B**) Lateral view showing the crown of spines anteriorly. (**C**) Ventral view. (**D**) Posterior view.

and at the distal end of the ventro-median process. The parasphenoid is slightly curved in intermediate sizes and completely curved and ossified in the juvenile specimen.

The pterosphenoid is in the postero-dorsal corner of the orbit, dorsally sutured to the frontal ventro laterally and posteriorly to the sphenotic and prootic (Fig. 3C). The ventral edge is concave (Fig. 3B) and wider anteriorly, and forms a median process with a flat anterior facet (Saeed et al., 2006). The mid-section begins to ossify ventrally at 9.77 mm SL and is fully ossified in the mid-section by 13.82 mm SL, with an increasing extension of bone towards the anterior and posterior ends in the juvenile. The basisphenoid and sclerotic bones are absent in all specimens examined.

Otic region

The parietal (=postparietal of Schultze [2008]) is the largest bone of the otic region (Fig. 3A), is covered by the frontal anteriorly, and forms the anterior ridge and floor of the posttemporal fossa. It is sutured laterally to the sphenotic, overlaps the supraoccipital medially and the epiotic posteriorly (Figs. 2 and 3A). The parietal appears first at 11.14 mm SL along the chondral ridge with the frontal, and is in contact with the sphenotic and epiotic at 13.82 mm SL. This bone carries a few odontodes on its dorsal surface. The floor of the posttemporal fossa is not ossified in the juvenile specimen.

The sphenotic (=autosphenotic of Schultze [2008]) is sutured anteriorly to the frontal and pterosphenoid, dorso-medially to the parietal, and posteriorly to the pterotic bones (Fig. 3A–C). It bears a small tendon bony process oriented ventrally and lacks a sensory canal (Figs. 2 and 3B). Together with the pterotic bone, they form the socket of the hyomandibular condyle, with a pterotic capsule posteriorly and the base of the sphenotic process anteriorly (Fig. 3, B and C). Dorsal to this articulation is the otic sensory canal, two-thirds of which is fused to the pterotic, with the anterior third overlapping the sphenotic (Figs. 2 and 3A). The otic sensory canal is not connected to the preopercular or the infraorbital sensory canal, with only pore 6 anteriorly and pore 8 posteriorly, and has one or 2 odontodes at either end of the medial ridge (Fig. 3, A and B). The sphenotic and pterotic appear as small bones at 9.77 mm SL, the former around the base of the postorbital process and along the antero-medial edge between the prootic and pterosphenoid, and the latter posterior to the hyomandibular articulation. By 11.14 mm SL, all 3 bones have extended their ossification, and by 15.42 mm SL the sphenotic bone is extended under the frontal along the orbital rim and contacts the pterotic over the hyomandibular articulation. By 16.21 mm SL, the pterotic has reached the exoccipital medially and the sphenotic process projects ventrally, extending below the hyomandibular articulation. All bones are connected to each other in juveniles, with the otic sensory canal fully formed and only the parietal with odontodes.

The epiotic lies postero-laterally to the supraoccipital and postero-ventrally to the parietal, which overlaps it dorsally. This bone forms a wide ridge to which the posttemporal is connected and the ridge continues ventrally by the exoccipital (Fig. 3, A and D). The epiotic appears ossified at 9.77 mm SL in the area where it articulates with the posttemporal and ventrally along the ridge towards the exoccipital. By 16.21 mm SL, the epiotic has expanded and sutures with the parietal dorsally.

The prootic sutures to the pterosphenoid antero-dorsally, to the sphenotic dorsally, ventrally to the parasphenoid, and posteriorly to the pterotic, exoccipital, and basioccipital (Fig. 3, B and C). The prootic sutures its counterpart medially and forms the roof of the posterior myodome. A thin fan-like ridge extends antero-laterally from the ascending process of the parasphenoid and forms a trigeminal arch dorsally (Fig. 3, B and C). The large single trigeminal foramen is fully enclosed by the prootic (see Dyer, 1997:15). Ventrally, the prootic and basioccipital form a protruding cartilaginous surface that articulates with the pharyngobranchials 2 and 3. By 7.89 mm SL, the prootic is ossified at the center where the trigeminal arch and foramina are located. Ossification is extended medially towards its counterpart to form the posterior myodome roof and posteriorly towards the exoccipital at 9.77 mm SL, dorsally toward the sphenotic by 11.14 mm SL, and fully ossified in the juvenile.

Some elements of the otic region can be differentiated at 7.89 mm SL as thin plates of perichondral ossifications. By 31.16 mm SL, the parietal, sphenotic, prootic, and epiotic bones are almost completely ossified, but the pterotic is still in process of ossification. Extrascapulars are absent in the material examined and in adults.

Occipital region

The supraoccipital is located medially in the postero-dorsal part of the braincase, with a reduced supraoccipital process (Fig. 3, A, B, and D). The supraoccipital extends anteriorly under the median ends of the frontals and laterally under the parietals. The posterior part of the neurocranium, between the supraoccipital and the foramen magnum, remains cartilaginous in all specimens (Fig. 3, A and D). Postero-ventrally, the supraoccipital is separated from the epiotics by cartilage (Fig. 3, A and D). First hints of ossification are seen around the posterior border of the pineal organ concavity at 9.77 mm SL and it is more clearly ossified by 13.82 mm SL, with a visible supraoccipital process. It is almost completely ossified anteriorly under the frontals by 15.42 mm SL, laterally to parietals by 16.21 mm SL, and completed by

31.16 mm SL, except for the medial postero-ventral portion that remains cartilaginous.

The exoccipital is sutured dorsally to the epiotic, ventrally to the basioccipital, anteriorly to the prootic, and dorso-laterally to the pterotic (Fig. 3), forming the sides of the foramen magnum and also an articular surface for the first vertebra (Fig. 3B–D). Baudelot's ligament is attached to the exoccipital at the base of the articular process to the first vertebra and posterior to the foramina of nerves IX and X (see Dyer, 1997:18). By 7.89 mm SL, the exoccipital is clearly ossified in a flattened-hourglass shape, and by 9.77 mm SL, it is in contact with the basioccipital ventrally. By 11.14 mm SL, the condyle of the exoccipital to the first vertebra is ossified, and by juvenile size, the counterparts are separated dorsally by cartilage.

The basioccipital articulates posteriorly with the first vertebra (Fig. 3C). Anterior to this large circular condyle is a medio-ventral groove that forms the roof and lateral walls of the posterior myodome. It articulates dorso-laterally with the exoccipitals (Fig. 3D) and anteriorly with the prootic with which it forms the articulation with the pharyngobranchials. The basicranial region is the first part of the neurocranium to ossify, specifically, the basi- and exoccipital bones, the prootic, and parasphenoid by 7.89 mm SL. The intercalar is absent in all specimens, including adults.

Infraorbital sensory canal bones

The infraorbital canal is reduced to 2 bones, the lacrimal (infraorbital 1) and the infraorbital 2. The posterior rim of the lacrimal articulates with the lateral ridge of the preorbital region of the ethmoid cartilage. A wide dorsal lamina of the lacrimal projects towards the nasal and forms a bony separation between the nasal pores (Fig. 2). The anterior tip articulates with the lateral process of the ethmoid cartilage, posterior to the dorsal process of the maxilla and lateral to the anterior tip of the pars autopalatina (Fig. 2). A subnasal shelf projects medially under the nasal capsule and over the autopalatine. The first ossification appears along an antero-medial ridge at 9.77 mm SL and along a dorso-medial ridge (parallel to the preorbital process) by 11.14 mm SL, forming an *L*-shaped ossification. The ossification is almost complete by 16.21 mm SL.

Infraorbital 2 is a long laminar bone that extends postero-ventrally slightly below the eye and beyond the tips of the maxilla and premaxilla (Fig. 2), with a membranous sensory canal pore at either end. It appears first by 11.14 mm SL and is fully ossified by 16.21 mm SL. The infraorbital sensory canal has 3 membranous pores--a dorsal pore over the lacrimal, a ventral pore under infraorbital 2, and a middle pore between both infraorbital bones. Both infraorbitals carry a row of odontodes on either side of the sensory canal in the juvenile (Fig. 4A). The species lacks a dermosphenotic.

Oral jaws

The premaxilla is the largest element of the upper jaw with a reduced ascending process. The proximal end is laminar and convex (Figs. 2 and 4), where the odontodes are present in juvenile and adult specimens. Five or 6 conical oral teeth are confined along its antero-ventral rim. Two or 3 teeth are already present at 7.89 mm SL. Between the ascending processes is a small, ovoid rostral cartilage (Fig. 4B). The distal end of the alveolar arm of the premaxilla is rounded where it overlaps the lower jaw and lies medial to the maxilla (Figs. 2 and 4A). This bone is partially ossified at 7.89 mm SL and complete by 16.21 mm SL.

The dorsal process of the maxillary head is reduced to a dorsal crest that articulates with the anterior part of the lateral process of the ethmoid cartilage, the anterior tip of the pars autopalatina and the lacrimal (Figs. 2 and 4). This articular region of the maxilla has a well-developed ventral process that projects antero-medially towards the rostral cartilage. The shaft of the maxilla is slightly convex and wider postero-ventrally, extended slightly beyond the tip of the premaxilla (Figs. 2 and 4), and joined by ligament to the anguloarticular of the lower jaw. This bone is partially ossified at 9.77 mm SL and complete by 13.82 mm SL.

The dentary is the largest element of the lower jaw and has a disorderly row of about 20 small conical teeth along the anterior half of its dorsal rim (Fig. 4B), except at the symphysis (Fig. 4A, insert). The dentary and the anguloarticular form the coronoid process, with a very narrow spacing in between the 2 bones (Figs. 2 and 4B). Ventrally, the dentary houses the mandibular section of the sensory canal with 4 pores. It is partially ossified along the ventral shaft near the trajectory of the sensory canal at 7.89 mm SL and completely ossified at 9.77 mm SL.

The anguloarticular articulates with the internal surface of the ventral shaft of the dentary. It has a condylar articulation with the quadrate and a bony spur projected posteriorly below the mandibular articulation (Fig. 4B). This bone does not carry a sensory canal. A hook-shaped retroarticular is present on the postero-ventral corner of the lower jaw (Fig. 4). It appears first at 9.77 m SL and is disconnected from the anguloarticular in all larvae. Meckel's cartilage is fully developed by 9.77 mm SL and extends along the medial surface of the anguloarticular and dentary (Fig. 4B). The anguloarticular is clearly visible by 9.77 mm SL and is the last to fully ossify in the juvenile. The coronomeckelian is first seen at 15.42 mm SL and lies between Meckel's cartilage and the base of the anguloarticular (Fig. 4B). Odontodes are only present in the juvenile specimen, mostly on the ridges of the

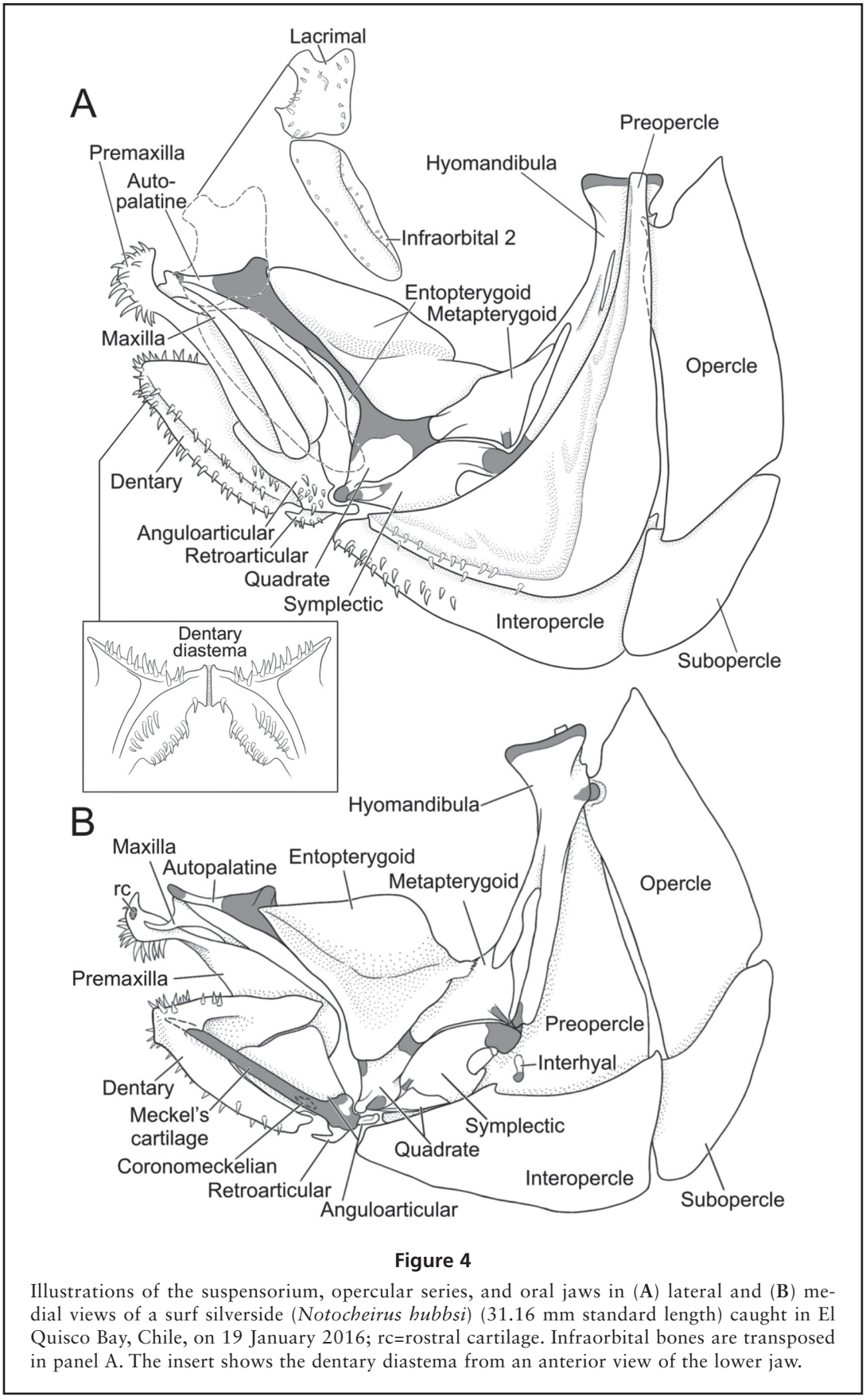

Figure 4

Illustrations of the suspensorium, opercular series, and oral jaws in (**A**) lateral and (**B**) medial views of a surf silverside (*Notocheirus hubbsi*) (31.16 mm standard length) caught in El Quisco Bay, Chile, on 19 January 2016; rc=rostral cartilage. Infraorbital bones are transposed in panel A. The insert shows the dentary diastema from an anterior view of the lower jaw.

mandibular sensory canals, but also present on the retroarticular and around the base of the anguloarticular (Figs. 2 and 4A).

Suspensorium

The elongated and slender hyomandibula is the largest element of the suspensorium, which articulates with a double-condyle head with the neurocranium. A posterior directed condyle articulates with the opercle (Figs. 2 and 4). The vertical shaft of the preopercle is connected by tissue to the lateral ridge of the hyomandibular shaft (Fig. 4A). Cartilage separates the hyomandibula from the symplectic (Fig. 4B). This cartilage articulates also with the cartilaginous posterior tip of the metapterygoid and the interhyal (Fig. 4B). An anterior oriented lamina of membrane bone of the hyomandibula articulates with the dorsal wing of the metapterygoid, forming an arch through which passes the hyomandibular nerve (Fig. 4). The shaft of the hyomandibula is mostly ossified at 7.89 mm SL, with a weak perichondral ossification of the symplectic, metapterygoid, and quadrate.

The quadrate articulates via a large condyle with the anguloarticular and has a posterior process that articulates ventrally with the anterior end of the horizontal shaft of the preopercle (Fig. 4B). The symplectic is large and articulates with the main body of the quadrate and its posterior process and dorsally with the metapterygoid (Figs. 2 and 4). The quadrate, metapterygoid, and symplectic are almost completely ossified in the juvenile specimen.

The entopterygoid supports the eye ventrally, and its lateral rim is folded ventrally and connected medially to the mid-section of the palatoquadrate bones and pars palatoquadrate in the juvenile (Fig. 4). The entopterygoid is joined anteriorly to the pars autopalatina and to its lateral ethmoid ligament, medially to the quadrate and pars quadrata in the mid-section, and posteriorly to the metapterygoid (Figs. 2 and 4B). This bone is absent at 7.89 mm SL, but present at 9.77 mm SL and fully ossified by 16.21 mm SL. An ectopterygoid is lacking in all specimens and is absent in adults.

The autopalatine is reduced to a small cone-shaped bone at the base of the pars autopalatina anterior process, with the most anterior tip cartilaginous, which articulates with the lateral process of the ethmoid cartilage (Figs. 2 and 4A). The posterior part of the autopalatine remains cartilaginous (pars autopalatina) and articulates with the ventral cartilaginous rim of the lateral ethmoid and via a ligament (Fig. 4B). The autopalatine is present only in the juvenile and adults.

Opercular series

The preopercle is boomerang-shaped, with almost a 90° angle between the vertical and the horizontal shaft. The longer vertical shaft is narrower dorsally than ventrally and attaches by connective tissue to the lateral side of the hyomandibular shaft (Figs. 2 and 4). The horizontal shaft equally attaches to the symplectic and posterior process of the quadrate. The preopercular sensory canal has 4 pores on the vertical shaft and 3 pores on the horizontal shaft, the latter shaft only with odontodes in the juvenile. The preopercle is most ossified at its angle at 7.89 mm SL and fully ossified at 9.77 mm SL.

The rhomboidal-shaped opercle articulates anterodorsally with a condylar articulation of the hyomandibula and attaches ventrally to the subopercle (Fig. 4B). The antero-dorsal process of the opercle lies between the preopercle and the hyomandibula (Fig. 4A). The subopercle connects medially to the ventral margin of the opercle and laterally to the posterior margin of the interopercle (Figs. 2 and 4). The dorsal half of the triangular-shaped interopercle lies medially to the preopercle with the dorsal margin indented in specimens 15.42, 16.21, and 31.16 mm SL (Fig. 4B), where the preopercular-ceratohyal ligament crosses over it. The interopercle connects via a ligament to the retroarticular anteriorly, medially to the posterior ceratohyal, and the posterior margin overlaps the subopercle. The interopercle has odontodes along the anterior half of the lateral ventral margin (Figs. 2 and 4A). Ossification of the opercle appears strongest at the condyle at 7.89 mm SL and is faintly visible ventrally and posteriorly, as are the subopercle and interopercle. The opercle is visibly ossified yet incomplete at 9.77mm SL, as are the subopercle and interopercle. The opercular series is fully ossified at 16.21 mm SL.

Branchial basket

Hyoid arch

The dorsal and ventral hypohyals are joined by connective tissue to each of their counterparts medially (Fig. 5). The dorsal hypoyal also articulates with the basihyal. The hypohyal shows first ossification at 9.77 mm SL as tiny superficial spines and the first perichondral ossification begins at 16.21 mm SL.

The anterior ceratohyal is the largest bone of the arch, separated by cartilage from the hypohyal and the posterior ceratohyal, but connects to the latter by a long bony strut along the medial and lateral surfaces (Fig. 5, A and B). The medial strut is already visible at 7.89 mm SL together with perichondral ossification. The posterior ceratohyal has a posterior shelf which articulates with the interhyal, and anteriorly is a short ligament that connects laterally to the interopercle. The posterior ceratohyal ossifies first at 9.77 mm SL, posteriorly where it articulates with the interhyal, and is mostly ossified in the juvenile.

The interhyal is a short tubular bone that connects the posterior end of the hyoid arch to the suspensorium at the hyomandibular-symplectic-metapterygoid junction

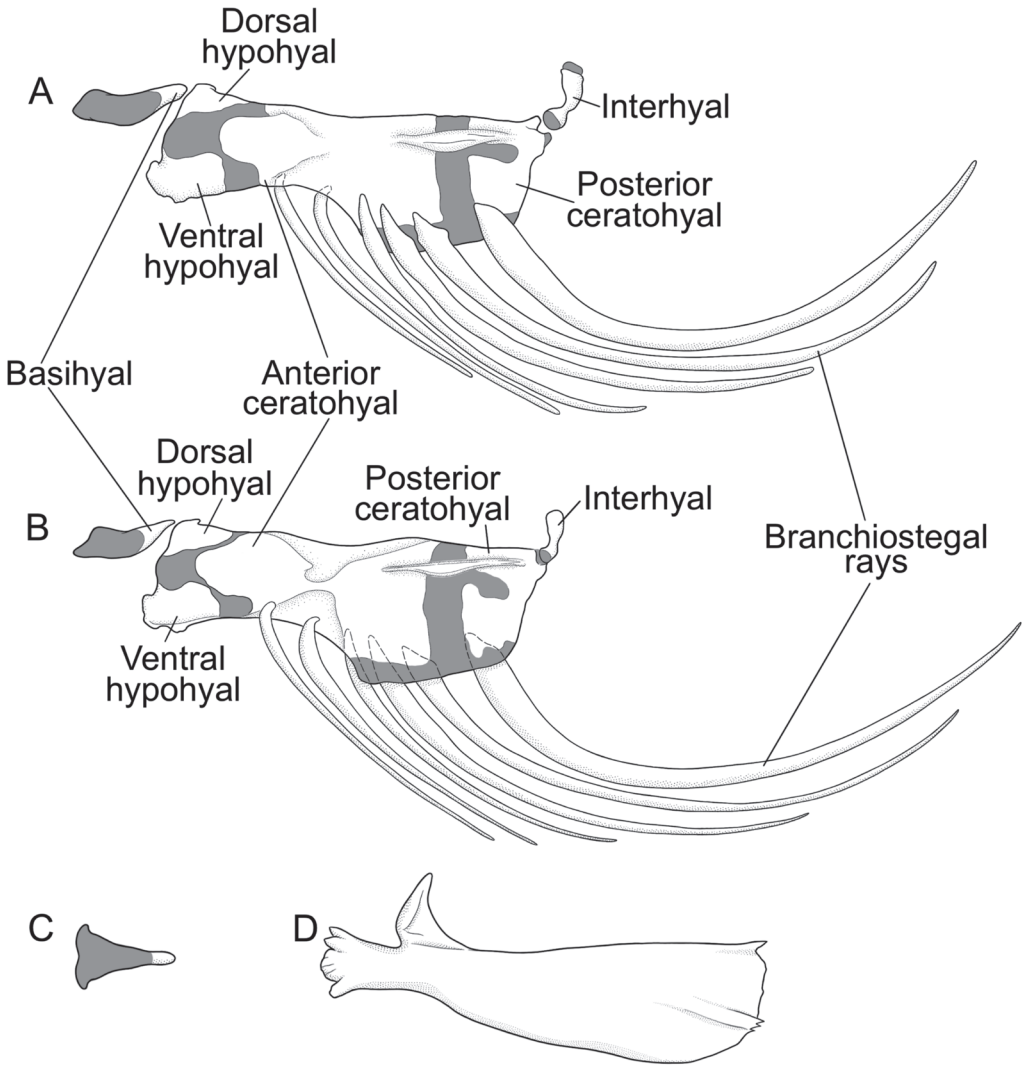

Figure 5

Illustrations of the hyoid arch of a surf silverside (*Notocheirus hubbsi*) (31.16 mm standard length) caught in El Quisco Bay, Chile, on 19 January 2016: (**A**) lateral view, (**B**) medial view, (**C**) dorsal view of the basihyal, and (**D**) lateral view of the urohyal.

(Figs. 4B and 5). The ossification is first observed at 13.82 mm SL.

The dorso-ventrally flattened basihyal is connected posteriorly to the dorsal hypohyals (Fig. 5, A and B). The anterior end is 3 times as wide as its posterior end with a concave to flat anterior margin (Fig. 5C). Ossification appears first at its posterior margin in the juvenile.

The urohyal is an elongated laminar bone about as long as the hyoid arch (Fig. 5D), that lies ventral to the basibranchial series. It has a slightly spatulate anterior process that is connected by 2 dorsal and 2 ventral ligaments to the hypohyals and a dorsal process that is joined by connective tissue to the anterior ventral surface of basibranchial 2. The dorsal rim of the median shaft and the dorsal and anterior bifid processes are first seen at 7.89 mm SL. Ossification progresses posteriorly with size, with the reduced dorsal process appearing ossified first at 15.42 mm SL and fully ossified at 16.21 mm SL.

There are 6 branchiostegals with the posterior ray the largest and supported by the posterior ceratohyal (Fig. 5, A and B). The remaining 5 are supported by the anterior ceratohyal, of which the shortest 2 anterior rays are joined to the medial side (Fig. 5, A and B). The branchiostegals are among the earliest dermal bones to ossify;

the 4 posterior rays are visible at 7.89 mm SL and all branchiostegals are completely ossified at 11.14 mm SL.

Gill arches

Basibranchial 1 is reduced to a small cartilaginous nodule anterior to basibranchial 2 (Fig. 6A). A space half the length of the basihyal is between the basihyal-hypohyal juncture and the basibranchials. Basibranchial 2 is anteriorly narrow to a point between the first hypobranchials and is extended posteriorly to the second hypobranchial articulation at the anterior end of basibranchial 3 (Fig. 6A). Basibranchial 3 is narrow anteriorly between the second hypobranchials, extends posteriorly to the third hypobranchial articulation and slopes under basibranchial 4. The diamond-shaped basibranchial 4 is cartilaginous and joined laterally by hypobranchials 3 and posteriorly to ceratobranchials 4 (Fig. 6A). Basibranchials 2 and 3 are partially ossified at 11.14 mm SL, and ossification is almost complete in the juvenile specimen.

Hypobranchial 1 articulates medially with basibranchial 2 and laterally to its corresponding ceratobranchial 1 (Fig. 6A). Hypobranchial 2 articulates with the anterior end of basibranchial 3 and hypobranchial 3 articulates with basibranchial 4, slightly dorsal to posterior end of basibranchial 3. Laterally, hypobranchials 2 and 3 articulate posteriorly with their corresponding ceratobranchials 2 and 3 and have a developed antero-ventral process. Ossification is first observed at 11.14 mm SL and is well ossified by 31.16 mm SL.

Ceratobranchials 1 to 4 are elongated bars, roughly of equal length, curved dorsally and articulated posteriorly with their corresponding epibranchials (Fig. 6A). Each ceratobranchial has a narrow central ridge with a laminar flange expanded ventrally towards the gill filaments. Dorsally, on either side of the central ridge are 2 rows of gill rakers, except ceratobranchial 4 that bears a single series of 7 spine-patches along the lateral side. Ceratobranchial 5 is the shortest of all ceratobranchials and bears the lower pharyngeal tooth plate. Its anterior half articulates medially to its counterpart (Fig. 6A). Ceratobranchial 5 is curved postero-laterally in the midsection roughly at a 30° angle and has a well-developed ventro-medial wing of membrane bone. The lower pharyngeal tooth plate has long conical teeth in the anterior section, followed by shorter teeth in the midsection, and along the postero-medial border there are larger and thicker unicuspid teeth (Fig. 6A). Ceratobranchials 1 through 4 are weakly ossified at 7.89 mm SL and well ossified at mid-bar at 11.14 mm SL. Ceratobranchial 5 and its associated tooth plate are well ossified at 7.89 mm SL.

Epibranchials 1 to 3 are cylindrical and of decreasing length posteriorly, with epibranchial 3 roughly one-half the length of the first and with an uncinate process proximally (Fig. 6, A and B). Epibranchial 1 lacks an uncinate process and an interarcual cartilage to epibranchial 2. Epibranchials 2 and 3 are joined to pharyngobranchials 2 and 3, respectively (Fig. 6, A and B). Epibranchial 4 is the largest of this series with a large dorsal process, a small subterminal uncinate process to epibranchial 3, and a wide subcircular cartilaginous articulation with pharyngobranchial 3 (Fig. 6, A and C). Epibranchials 2 and 3 are partially ossified at 15.42 mm SL and epibranchial 1 is first ossified at 16.21 mm SL. Epibranchial 4 has its dorso-lateral wing ossified at 7.89 mm SL and is fully ossified at 16.21 mm SL.

Pharyngobranchial 2 is vertically positioned and articulates dorsally to the neurocranium, wider ventrally, and fused to upper pharyngeal tooth plate 2, with a single row of 3 teeth (Fig. 6, A and C). Pharyngobranchial 3 is the largest bone of the upper series, with an antero-dorsal process that articulates with the neurocranium in tandem with pharyngobranchial 2, and a wider postero-dorsal extension that articulates with epibranchial 4 (Fig. 6, A and C). Pharyngobranchial 3 is fused to the larger upper pharyngeal tooth plate 3 with long conical teeth laterally and medially with strong, flattened, and asymmetrically bicuspid teeth (Fig. 6C). These bones are observed partially ossified and with teeth at 7.89 mm SL. Pharyngobranchial 1 is absent, not epibranchial 1 as mentioned by Saeed et al. (2006).

Gill rakers are only present on the first hypobranchial and ceratobranchial (Fig. 6D). The lateral row of the first branchial arch has gill rakers with a wide base, laminar and tapering distally, and a thicker medial rim with a single row of up to 10 spines on the internal face. In the juvenile, 10 gill rakers are counted; the first is a very small raker at the angle between upper and lower branches, rakers 2 to 4 are successively longer, rakers 5 through 7 are the longest, and rakers 8 to 10 decrease in length anteriorly (Fig. 6D). The first gill rakers (6) are observed at 9.77 mm SL in the middle section of the ceratobranchial.

Axial skeleton

The 7 cleared and stained specimens have 39–42 vertebrae in total (including the urostyle), 12–13 precaudal and 25–29 caudal vertebrae. The anterior 6 or 7 precaudal vertebrae have a broad laminar neural spine, reduced in width posteriorly. The posterior 5 vertebral centra, preural centra 2 to 6, have elongated neural and haemal spines with cartilaginous distal ends, supporting the dorsal and ventral procurrent rays of the caudal fin (Fig. 7A). Preural centrum 2 articulates posteriorly with the urostyle and has a well-developed neural arch fused to the neural spine which in turn articulates with the posterior-most procurrent ray. The haemal arch is equally well developed and has a wider haemal spine that articulates with the last 2 principal rays.

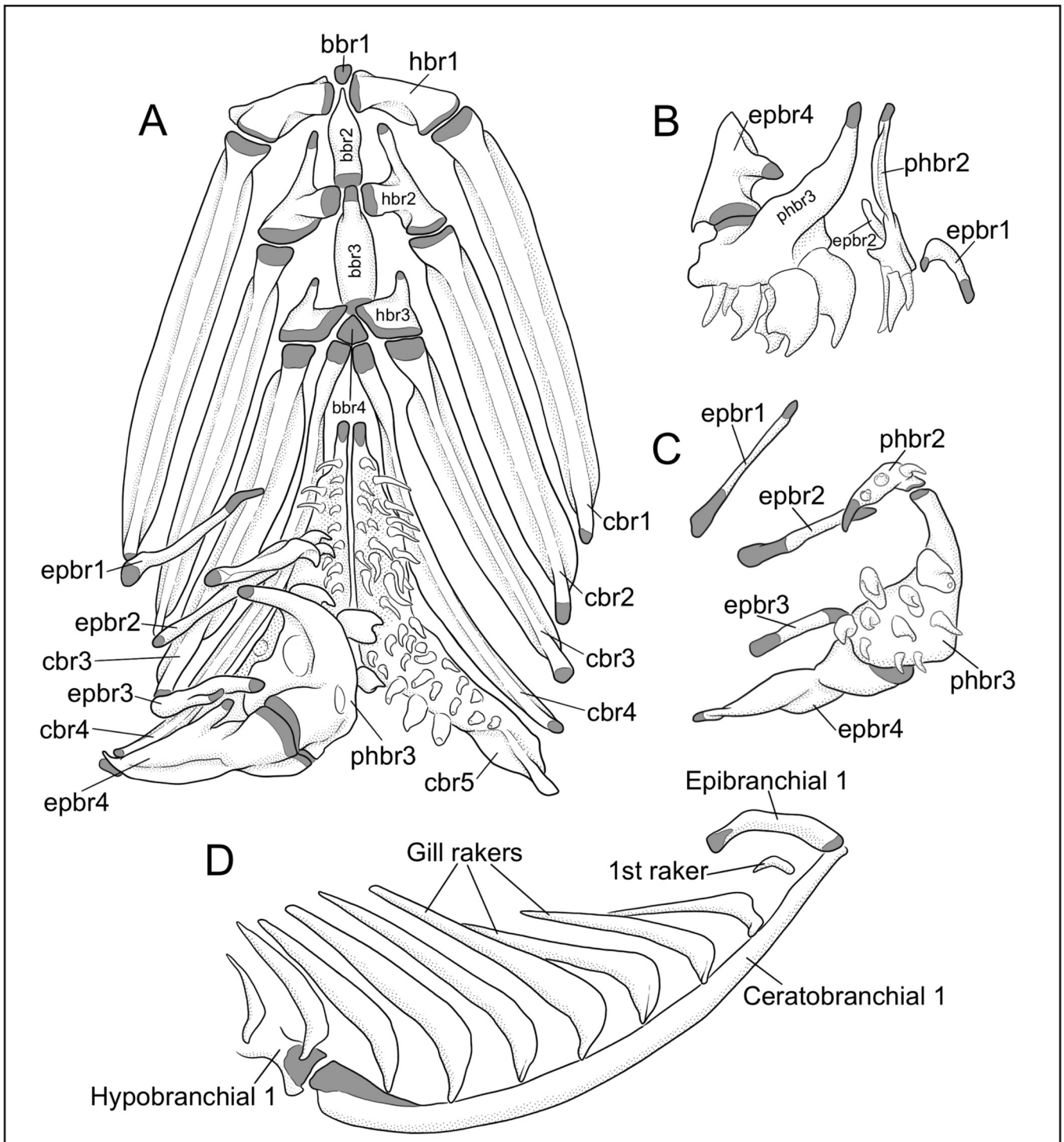

Figure 6

Illustrations of branchial arches of a surf silverside (*Notocheirus hubbsi*) (31.16 mm standard length) caught in El Quisco Bay, Chile, on 19 January 2016; bbr=basibranchial; cbr=ceratobranchial; epbr=epibranchial; hbr=hypobranchial; phbr=pharyngobranchial. (**A**) dorsal view with the gill rakers removed, (**B**) medial view of the upper pharyngeal jaws, (**C**) upper arches of the right side in ventral view, and (**D**) lateral view of gill rakers on the first gill arch on the left side.

The vertebrae are formed by an autocentrum fused to the dorsal and ventral arcocentra, each with their corresponding remnant basidorsal and basiventral cartilaginous arcualia (still visible at 11.14 mm SL; Fig. 7C). At 7.89 mm SL, only the first 4 vertebrae are partially ossified, of which only the first vertebra has a very short neural spine. Neural arches of vertebrae 2 to 4 have no spine visible. Vertebrae 5 to 7 have incomplete neural arches and lack spines, due to damage. The neural arches, from vertebrae 8 to 14, have their distal halves cartilaginous and continuous with the neural spine. From vertebrae 15 caudad, neural arches only have a single cartilaginous spine extending dorsally from the fusion of the dorsal arcocentra. A remnant of the basidorsal arcualia is visible at the base of all larval neural arches (Fig. 7). The centers of ossification of the vertebrae begin with the dorsal arcocentra around the basidorsal arcuale and the gradual ossification of the autocentrum and the external sheath around the notochord. From vertebrae 4 caudad, the ventral arcocentra around the basiventral arcuale are also ossified, which give rise to the parapophyses that by vertebra 12 are directed ventrally and complete the first haemal arch. Preural centrum 2 has 2 neural arches, each with a cartilaginous neural spine. Ventrally, there is a single haemal arch with a broad cartilaginous rod as a haemal spine. Haemal arches are present from vertebra 14 caudad and are non-cartilaginous (except for the basiventral arcuale remnants), with a single cartilaginous haemal spine extending distally from the fusion of both ventral arcocentra.

At 9.77 mm SL, the first 7 vertebrae are partially ossified (autocentrum and dorsal arcocentra) and the first 4 have the initial stages of the broad laminar neural spines. Vertebrae 6 and 7 have non-ossified neural spines extending distally from a cartilaginous base where both dorsal arcocentra meet. Vertebral centra 8 and caudad are not ossified, with cartilaginous neural and haemal spines (Fig. 7B). The neural and haemal arches are completely ossified, except for the remnants of the basidorsal and basiventral arcuale. The first haemal arch is formed on vertebrae 12 and the first haemal spine on vertebrae 15. The 4 posterior-most vertebrae have broader neural and haemal cartilaginous spines. Preural centrum 2 has a single neural arch at the anterior end of the centrum and, posterior to its cartilaginous spine, a cartilaginous rod not attached to the centrum (Fig. 7B). Four cartilaginous ribs are observed connected to the parapophyses of vertebrae 3 to 6.

At 11.14 mm SL, the anterior 13 vertebrae are partially ossified (autocentra, dorsal, and ventral arcocentra) with weaker ossification posteriorly as in 9.77 mm SL, but it also has the final 23 caudal vertebrae partially ossified with increased ossification posteriorly. All caudal vertebrae have cartilaginous neural and haemal spines. Preural centrum 2 has 2 neural arches, each with a cartilaginous spine, but only the anterior dorsal arcocentrum is partially ossified (Fig. 7C). The haemal arch is partially ossified with a cartilaginous spine. The autocentra are faintly ossified from vertebra 22 caudad, however the dorsal and ventral arcocentra are slightly ossified at the base of the arches (around the remnants of the basidorsal and basiventral arcuale) throughout the entire length of the axial skeleton. The first 5 vertebrae have broad laminar neural spines, and the remainder of the spines are cartilaginous proximally. Seven cartilaginous ribs are joined to the parapophyses of vertebrae 3 to 9.

Specimens 13.82–16.21 mm SL (Fig. 7, D and E) have all vertebral centra and neural arches completely ossified, though spines partially so, including the juvenile. These specimens have 8–10 ribs, proximally ossified and distally cartilaginous; the anterior 4 to 6 ribs are joined to the fused dorsal and ventral arcocentra and the posterior 4 are successively placed more ventrally on the parapophyses. The juvenile has 11 ribs; the first rib is short, connected to the parapophysis and centra of vertebra 2, not reaching the pectoral girdle. This first short rib is absent in the 6 larval specimens. Intermuscular bones are absent.

Paired fins

Pectoral girdle and fin

The posttemporal has a pointed dorsal process which articulates with the epiotic and a wider postero-ventral process which articulates with the cleithrum (Fig. 8). This bone lacks a ventral process (anterior process in Dyer [1997]) that attaches to the exoccipital and lacks a sensory canal. The posttemporal bone appears faintly at 9.77 mm SL and is fully ossified at 16.21 mm SL.

The cleithrum is the largest element of the pectoral girdle and is the first to develop. The dorsal wing of the cleithrum is pointed and its antero-dorsal surface articulates with the posttemporal (Fig. 8, A and B). The scapula and coracoid are joined to the medial face of a laminar flange extended posteriorly (Fig. 8, A and B). The ventral end of the cleithrum is spatulate in shape and sutured to its counterpart along the ventral midline as a dentate *sutura dentata*. This bone appears as a slender rod of bone at 7.89 mm SL and is gently curved at 13.82 mm SL and over.

The postcleithrum is a single long rib-like bone that articulates dorsally to the internal face of the coracoid (Fig. 8, A and B). Its ventral extension is slightly wider where it is sutured to its counterpart along the ventral midline as a slightly dentate *sutura dentata*. A partially ossified postcleithrum is present at 9.77 mm SL and is fully formed at 16.21 mm SL.

The scapula is the dorsal bone with the scapular

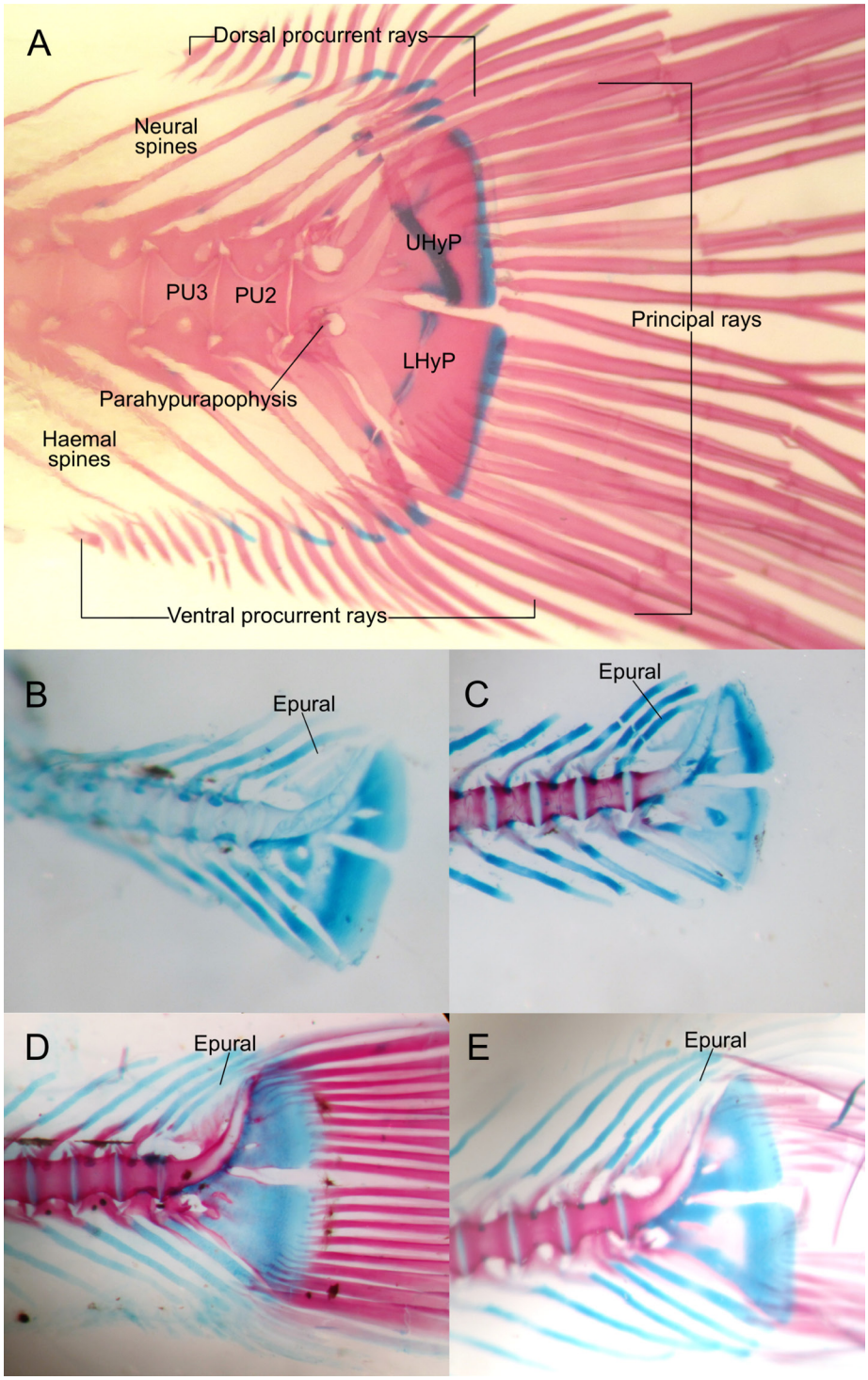

Figure 7

Photographs of the cleared and stained caudal fin of 4 surf silverside (*Notocheirus hubbsi*) specimens caught in El Quisco Bay, Chile; LHyP=lower hypural plate; UHyP=upper hypural plate. (**A**) Juvenile specimen (31.16 mm standard length [SL]) caught on 19 January 2016 with fractured hypural plates and neural spines of preural centrum (PU) 2 and PU3. (**B**) Larval specimen (9.77 mm SL) caught on 11 November 2015. (**C**) Larval specimen (11.14 mm SL) caught on 4 November 2015 with fractured epural and neural spines of PU2 and PU3. (**D**) Larval specimen (13.82 mm SL) caught on 10 December 2015. (**E**) Larval specimen (15.42 mm SL) caught on 11 November 2015.

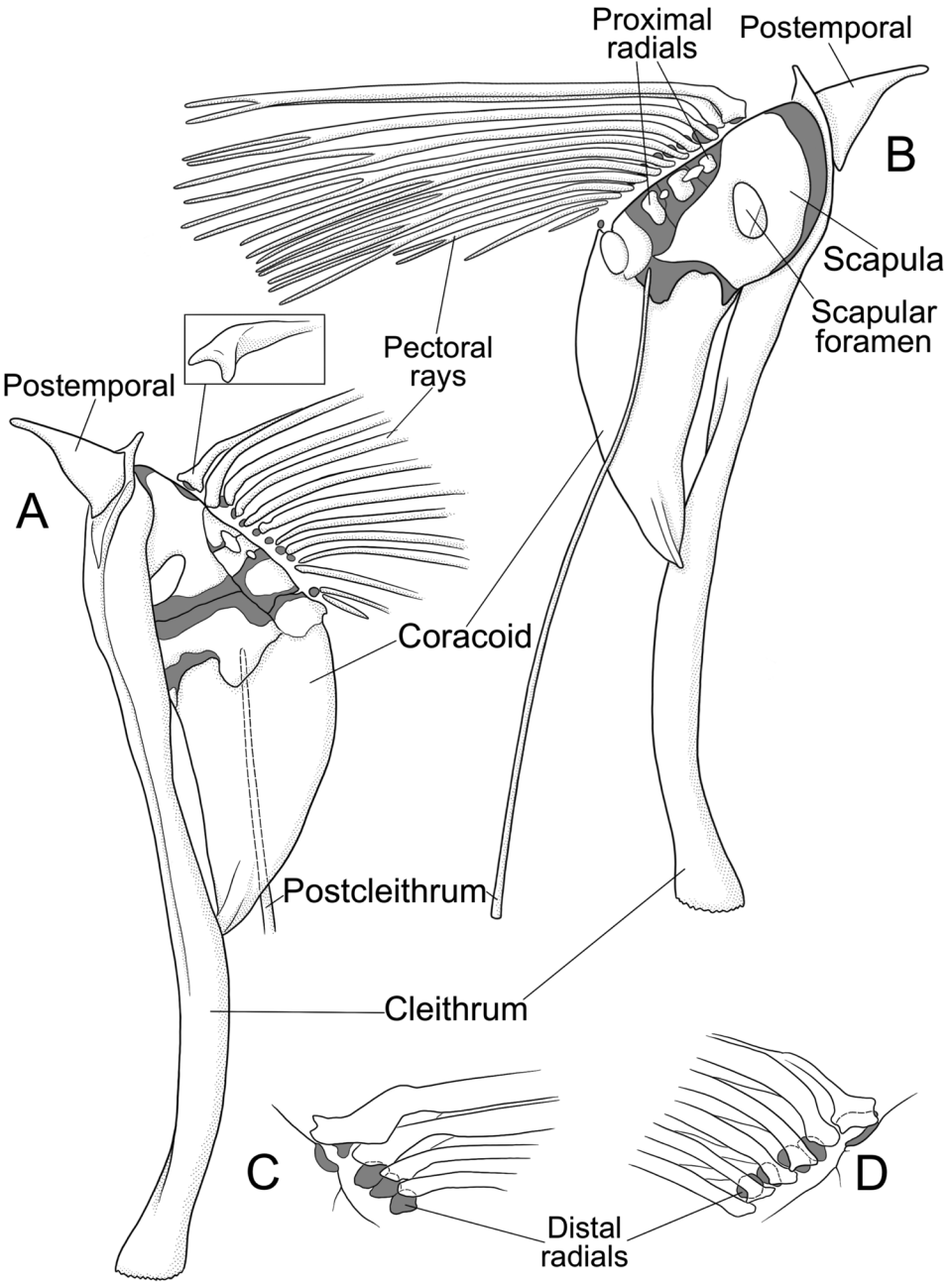

Figure 8

Illustrations of pectoral girdle and fin of a surf silverside (*Notocheirus hubbsi*) (31.16 mm standard length) caught in El Quisco Bay, Chile, on 19 January 2016. (**A**) Lateral view, with postcleithrum underlying the coracoid. The insert shows the detail of the first pectoral fin ray in dorsal view. (**B**) Medial view. (**C**) Detail of the first pectoral fin rays in lateral view. (**D**) Detail of the first pectoral fin rays in medial view.

foramen fully enclosed. It articulates along its ventral cartilaginous rim to the coracoid, both of which are joined anteriorly to the cleithrum (Fig. 8, A and B). The scapula is above the horizontal septum and the first 3 proximal radials articulate with its posterior margin. The initial ossification is observed at 15.42 mm SL where it articulates with the most dorsal fin ray.

The coracoid is widest at its articulation with the scapula and extends to the posterior margin of the fourth radial with which it is fused. It is tapered ventrally in a

Y-shaped process and joined to the medial surface of the cleithrum (Fig. 8B). The coracoid is slightly ossified along its posterior rim at 11.14 mm SL and is partially ossified along the anterior and posterior margins at 16.21 mm SL.

The first proximal radial is the smallest of the series and sutured to the posterior edge of the scapula, with a fenestra between it and the second radial. The second radial is joined to the scapula by cartilage. A small foramen is present between the second and third radial. The third radial attaches to the scapula-coracoid suture and is tightly attached to the fourth and largest radial, which overlaps medially the posterior end of the coracoid (Fig. 8B). Radials are faintly visible at 7.89 mm SL and clearly visible at 9.77 mm SL as separate elongated cartilages, but appear shorter and fused to each other in the juvenile, when the initial ossification is observed. The distal radials are all cartilaginous and the supracleithrum and dorsal postcleithrum are absent in all specimens (Fig. 8).

Each of the 11 pectoral fin rays (first unbranched and 10 branched) are associated with a distal radial and articulate with the scapula and proximal radials (Fig. 8, A and B). The leading first fin ray has a wider and robust medial branch that saddles the posterior rim of the scapula with which it articulates via a ligament with an apophysis on either side (Fig. 8A, insert). The first distal radial is fused to the enlarged medial hemitrich of the first fin-ray and remains cartilaginous in the juvenile specimen. The first free distal radials are enlarged. Subsequent distal radials decrease in size ventrad. The distal radial of the eleventh fin ray is the only one not located between the hemitrichs of the rays (Fig. 8, A and B). The first fin ray is visible at 7.89 mm SL, however at 9.77 mm SL it is only partially ossified with a cartilaginous element at the base of the fin-ray that articulates with the scapula (Fig. 8, C and D). Distal radials appear first at 15.42 mm SL and all are present in the juvenile.

Pelvic girdle and fin

The basipterygium and fin rays (Fig. 9) are present only in the juvenile specimen and are completely formed and ossified. The pelvic girdle and fins are missing in all larvae due to damage caused by megalopa evisceration during capture.

In lateral view, the pelvic bone has a roughly triangular shape with an elongated dorsolateral process that is connected to rib 4 (Fig. 9A). The anterior margin is rounded and meets ventrally at the midline with its counterpart bone, with which it is tightly joined to form a ventral keel (Fig. 9B). Dorsal to the bony keel is a large pelvic foramen traversed by medial muscles to the lateral hemitrichs of the pelvic fin. The median processes posterior and dorsal to the pelvic foramen, are tightly sutured and overlap each other with a short posterior process extended from the dorsal part of the symphysis (Fig. 9C). This bone lacks the anterior process with which the lateral and medial plates are associated in other atheriniforms. Two distal radials, one pelvic splint (a single hemitrich), and 5 rays are present (Fig. 9, B and C), reaching posteriorly to the vent (Fig. 1).

Median fins

A single dorsal fin is present with 2 short procurrent rays (Arratia, 2008), followed by 16 segmented rays, over the mid-section of the anal fin. Each dorsal pterygiophore has a bar-like proximal-middle radial and a round cartilaginous distal radial which is embraced by the hemitrichs of a single fin ray, except for the last pterygiophore which has an elongated distal radial that supports 2 small fin rays (Fig. 10A). The proximal ends of the pterygiophores do not insert deeply into the vertical septum between the neural spines. There are one to 3 pterygiophores inserting between the neural spines, with 2 as the most observed pattern. The second pterygiophore is the largest in the series. The first dorsal fin and its pterygiophores are absent.

The dorsal and anal fin elements seem to develop simultaneously. At 7.89 mm SL, the cartilaginous pterygiophores of both fins are faintly visible, though the middle pterygiophores appear to be more stained than the anterior or posterior ones. In the 9.77–16.21 mm SL specimens, the distal radials and pterygiophores are progressively more robust, but all unossified. In the juvenile specimen, the pterygiophores are partly ossified, the distal radials remain cartilaginous, and the rays are ossified. The anterior proximal radials are more ossified than the posterior ones.

The anal fin is longer with 2 procurrent rays and 30 segmented rays. The first procurrent ray is very short and associated directly with the proximal-middle radial. The second procurrent ray has a distal radial (Fig. 10B). The first anal pterygiophore is the largest of the series and is attached dorsally to the anterior surface of the first haemal spine. Ventrally, it articulates with 2 small procurrent rays, 2 distal radials, and an unbranched segmented ray. Each anal pterygiophore is formed by a bar-like proximal-middle radial with a rounded cartilaginous distal radial associated with a single fin ray, except the first and last pterygiophores. The posterior-most proximal radial has an elongated distal radial that supports 2 small rays (Fig. 10B). The anterior 3 pterygiophores insert deeper between the haemal spines to about one-third of their length. As in the dorsal fin, there are between one and 3 pterygiophores inserting between the haemal spines, with 2 pterygiophores being the most frequent pattern.

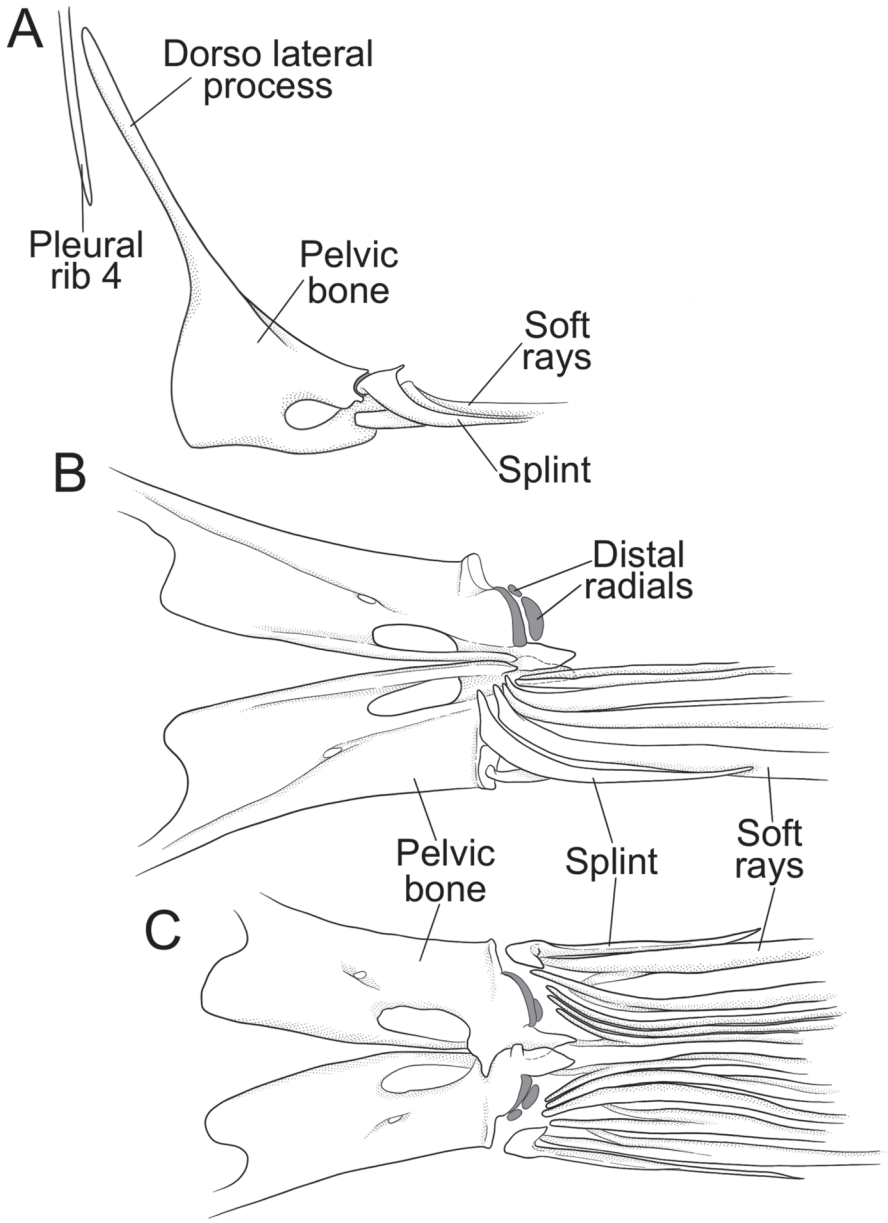

Figure 9

Illustrations of the pelvic girdle and fin in (**A**) lateral (left side), (**B**) ventral, and (**C**) dorsal views of a surf silverside (*Notocheirus hubbsi*) (31.16 mm standard length) caught in El Q uisco Bay, Chile, on 19 January 2016.

Caudal fin

The juvenile specimen (31.16 mm SL) has 18 principal rays, and 11 dorsal and 16 ventral procurrent fin rays (Fig. 7A). The upper and lower hypural plates support 9 principal rays each. The upper plate is a compound element consisting of the uroneural fused to the urostyle, to which hypurals 3–5 are fused. The lower plate consists of the parhypural and hypurals 1 and 2. Both hypural plates are fused to the urostyle which articulates with preural centrum 2 of the axial skeleton. The urostyle is assumed herein to be the fusion of 2 ural centra (Thieme et al., 2021), as it is fully formed in the smallest specimen (7.89 mm SL). The parhypural is fused to the centrum, has a well-developed parhypurapophysis, and the foramen in the lower hypural plate marks its anterior end. Its arch

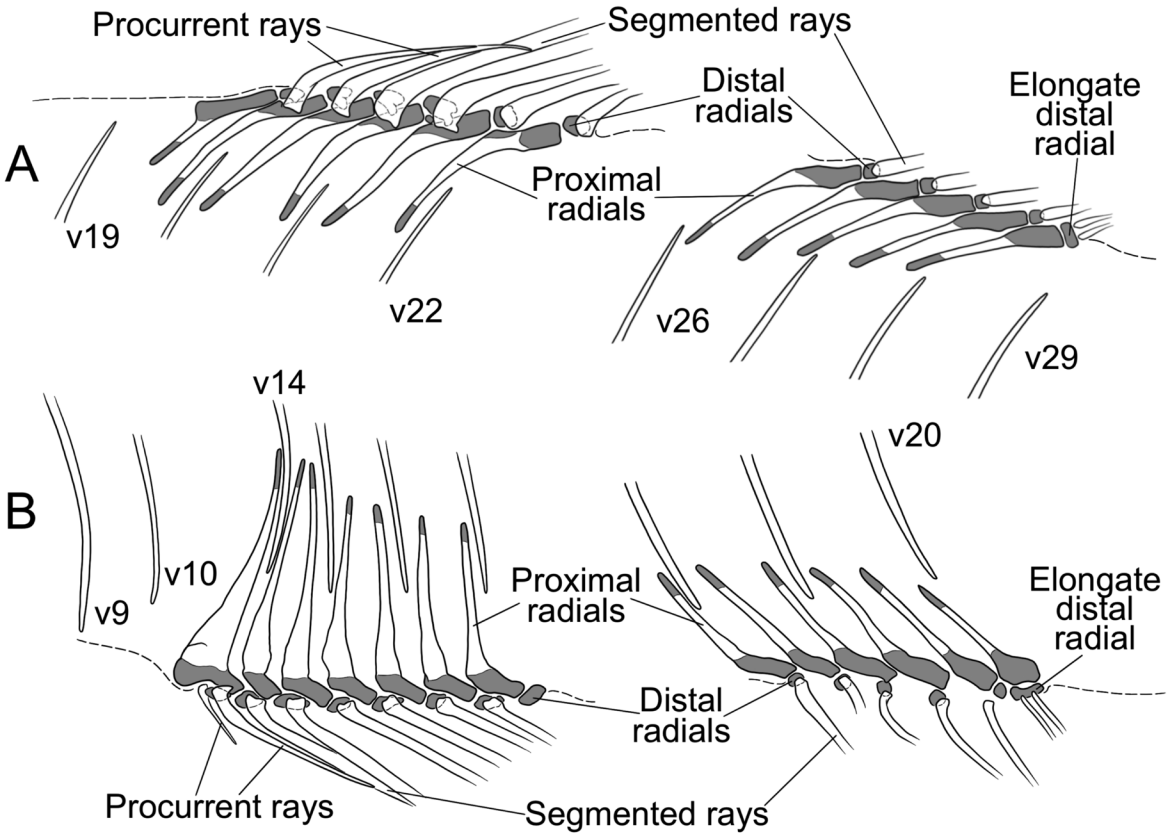

Figure 10

Illustrations of the (**A**) dorsal and (**B**) anal median fins of a surf silverside (*Notocheirus hubbsi*) (31.16 mm standard length) caught in El Quisco Bay, Chile, on 19 January 2016, detailing the anterior and posterior sections only; v=neural and haemal-spine tips of numbered vertebrae.

is fused to the centrum, as are all ossified haemal arches fused to the autocentra in the caudal vertebrae.

The absence of an epural in the juvenile and adults is a diagnostic feature of this species (Dyer and Chernoff, 1996; Saeed et al., 2006). However, larval specimens (9.77–15.42 mm SL) have a median cartilaginous rod above and anterior to the uroneural (Fig. 7B–E). This larval epural is interpreted as a detached neural spine (sensu Schultze and Arratia, 1989*)* of the posterior neural arch of preural centrum 2, the latter still visible at 7.89, 11.14, and 15.42 mm SL (Fig. 7, C and E). Both the epural and posterior neural arch are absent in specimens 16.21 and 31.16 mm SL (Fig. 7A).

The principal rays are partially ossified at 9.77 mm SL with the middle rays more so than the dorsal and ventral rays, and all completely ossified at 13.82 mm SL. The most posterior procurrent rays are only slightly ossified at 16.21 mm SL and fully ossified in the juvenile. The dorsal procurrent rays are supported by the tips of the neural spines of preural centra 2 through 6 and the ventral procurrent rays are supported by the haemal-spine tips of preural centra 2 through 7 (Fig. 7A). The procurrent rays are faintly visible at 13.82 mm SL (Fig. 7D), with a more developed ossification in a posterior to anterior progression at 15.42 (Fig. 7E) and 16.21 mm SL. All procurrent rays are completely ossified in the juvenile specimen (Fig. 7A).

At 7.89 mm SL, 5 cartilaginous elements posterior and ventral to the flexed notochord are present. The dorsal-most hypural is greatly reduced and the other 2 hypurals of the upper plate are separated. The largest cartilaginous element ventral to the diastema corresponds to the fusion of the distal two-thirds of the parhypural and hypurals 1 and 2. These are clearly separate elements proximally. At 9.77 mm SL, the fusion of the lower cartilaginous plate is developed to roughly three-fourths its length with 2 foramina. The upper plate consists of hypurals 3, 4, and 5. A large foramen marks the border be-

tween hypurals 3 and 4 (Fig. 7B) which persists to the juvenile stage (Fig. 7A). At 11.14 mm SL (Fig. 7C) the upper and lower plates are almost fully fused and the parhypurapophysis is developed.

Scales

The head and body are covered with spinoid scales only in the juvenile and adult specimens. No scales are seen in larval specimens. The head is bristly in juveniles and adults with or without odontodes, with non-imbricated spinoid scales of varying shape from snout to nape, the cheek, opercular bones, base of the jaws, and pre-pectoral fin area (Figs. 1 and 11A). Body scales are dorsoventrally oblong, with anterior and posterior margins smooth and posterior margin curved laterally, focus not visible, circuli in anterior field, and with 3 to 6 lateral spines in middle to posterior field (Fig. 11, B and C). According to Saeed et al. (1994), this type of scale is unique among teleosts; it also was not reported by Roberts (1993) for any atherinomorph or by Bräger and Moritz (2016) for any of the Mediterranean teleosts.

Discussion

Most of the comparative osteological studies of atheriniforms known to us have dealt with adult specimens exclusively. Exceptions are Richter and Moritz (2017) and Thieme et al. (2021). Thus, our analysis of the osteological development of *Notocheirus* differs from previous studies (Rosen, 1964; Said, 1983; Saeed et al., 1994; Dyer and Chernoff, 1996; Saeed et al., 2006) and needs to be further elaborated.

There are several bones that are either reduced in size or absent in *Notocheirus*. Bones of the head that are greatly reduced in size are the autopalatine (Figs. 2 and 4), basibranchial 1 (Fig. 6A), and the lack of the anteroventral process of the posttemporal (Fig. 8). The first gill raker (at the angle between upper and lower branches) is very small (Fig. 6D), while in atherinopsids it is the longest (Dyer, 1997; Mancini et al., 2016, fig. 13).

Bones that are lacking in the head are the vomer, mesethmoid, basisphenoid, dermosphenotic, extrascapular, intercalar, ectopterygoid, pharyngobranchial 1 (erroneously identified as epibranchial by Saeed et al. [2006]), and gill rakers on the upper branch or epibranchial 1. Based on the character descriptions of Dyer and Chernoff (1996), the absence of the vomer is unique among atheriniforms; the mesethmoid is also absent in *Neosthus*, Pseudomugilidae, *Craterocephalus,* and *Odontesthes*; the intercalar is missing in atherinopsids, *Iso*, *Dentatherina,* and Phallostethidae; the ectopterygoid is also absent in pseudomugilids and *Basilichthys*. Among the atheriniforms, *Notocheirus* shares the presence of the parietals only with atherinopsids. These characters are potentially diagnostic for the *Notocheirus* relationship within Atherinopsidae, as first proposed by Bloom et al. (2012). *Notocheirus* and *Iso* share the lack of the supracleithrum, the elongation of the cleithrum and postcleithrum, and the dorsal position of the pectoral fin, indicating a possible sister-group relationship. The dorsal postcleithrum is also absent in *Iso* and many other atheriniforms.

Our hypothesis is that the tear-drop shape of this species is due to a relative shortening of the ethmoid region and branchial basket, together with a contrasting increase in depth of the braincase, pectoral girdle, and a dorsal positioning of the pectoral fin. A morpho-geometric study may be able to detect these apparent growth patterns and provide a more general explanation to the reduction, absence, or lengthening of bones in specific regions of the head and body. The first dorsal fin is absent in all stages of development observed and is unique to *Notocheirus* in Atheriniformes.

Head

The premaxillary dorsal process is described by Rosen (1964:227) in his diagnosis of Isonidae as a "swollen symphyseal part to which clustered upper jaw teeth are attached." This feature, however, is restricted to *Notocheirus* only and is 2 independent characters: the "teeth-like appendages on scales and head" and the "swollen premaxilla symphysis" (Said, 1983: tables 12 and 13). Saeed et al. (2006:40, 41) described the "premaxilla bearing laterally-placed teeth" in *Notocheirus* and reiterated the premaxillary symphysis being "bullous" with a unique distribution of premaxillary teeth. However, the premaxillary dorsal process is not inflated, but a thin convex lamina with a median edge that provides a wide attachment to its adjoining counterpart, dorsal to the rostral cartilage. Furthermore, our observation is that the cluster of teeth on the dorsolateral surface of the premaxilla are in fact not oral teeth but instead odontodes or dermal denticles as in *Atherion* and *Denticeps* (Sire and Allizard, 2001), which are present only on dermal bones of the head in adults. Larval specimens have oral jaw teeth along the ventral edge of the premaxilla from 7.89 mm SL and up. These "teeth on the premaxillary facet" are absent in larval specimens, in the juvenile specimen (30.77 mm SL) without odontodes, and in some adult specimens examined by Dyer (2000, 2006). These juvenile and adult specimens without odontodes have their corresponding teeth on the oral jaws. Presence of odontodes in *Atherion* is suggested to be unique to atherinomorphs by Sire and Allizard (2001). This character was previously described for these species in Dyer and Chernoff (1996). A comparison of their structure and dental

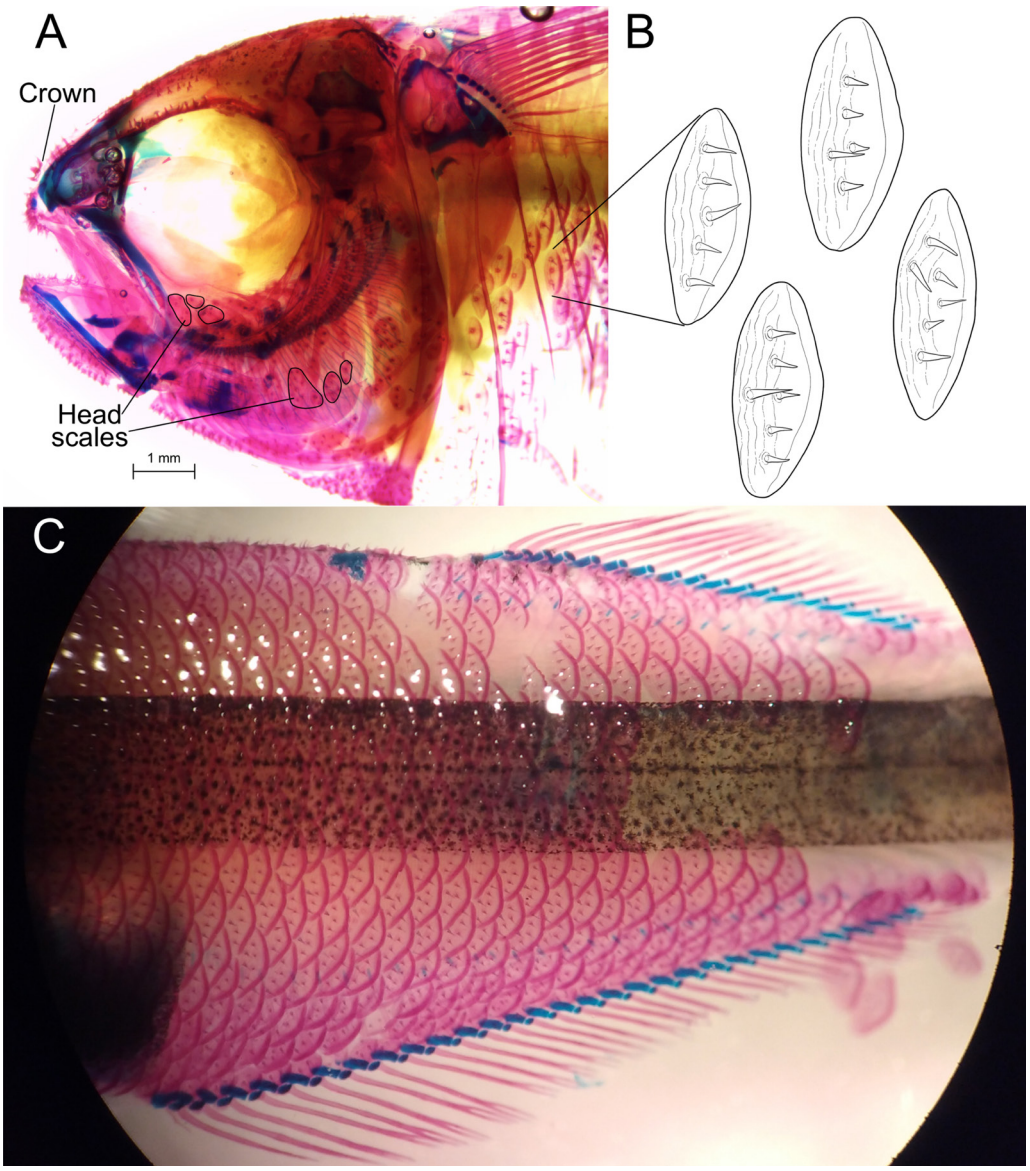

Figure 11

Lateral view of the scales of a surf silverside *(Notocheirus hubbsi)* (31.16 mm standard length) caught in El Quisco Bay, Chile, on 19 January 2016. (**A**) Photograph of the head (outlined) and body scales. (**B**) Illustrations of body scales. (**C**) Photograph of the body scales and dorsal and anal fins.

nature with *Notocheirus* is of interest to determine any atheriniform novelties.

The crown of spines is a cluster of odontodes joined to each other in a circular pattern not connected to the premaxillary dorsal process or any other dermal bone of the snout (Figs. 2 and 3, A and B). This disconnected odontode formation is quite noticeable in the cleared and stained specimens (Fig. 11A) and is described for the first time herein; it is absent in odontode-free specimens examined so far. The occurrence of odontodes in juveniles and adults, and this crown of spines on the snout, requires further study when more specimens are made available to determine whether it is a case of intraspecific variation (e.g., sexual dimorphism) or a relevant identification character at the species level.

The pattern of supraorbital sensory canal pores on the frontal bone was first studied by Gosline (1949) as a systematic feature for Cyprinodontiformes. The pattern in

Notocheirus was confirmed herein to share a relatively derived pattern with Atherinopsinae, in which the fifth pore is oriented medially instead of laterally as in other atheriniforms (Dyer, 1997:11, fig. 10d). The pores may vary significantly in their position anteriorly or posteriorly, but the direction of the pore opening seems to be conserved enough to propose homology of the pores. Such is the case of pore 5, which is oriented laterally in atheriniform outgroups and Old World silversides. The derived medial orientation of all atherinopsines and *Notocheirus* (Fig. 3A), is a character in partial support of the genomic-based placement of *N. hubbsi* in the atherinopsid family, but not in support of its sister group relationship with Menidiinae (Bloom et al., 2012; Campanella et al., 2015).

The parasphenoid is a straight bone in early larval stages 7.89–9.77 mm SL, curved between the ethmoid and the otic regions at 11.14–16.21 mm SL, and greatly curved in the juvenile. This characteristic curvature of the parasphenoid in late larvae and juveniles (Fig. 3B) seems to be a product of the greater depth of the braincase relative to the ethmoid region, related to the increased depth of the body at the pectoral-fin origin and, hence, the tear-drop shape of the body. Another unique feature within atheriniforms is the parasphenoid tunneling through the ethmoid cartilage at the preorbital region, appearing on the ventral surface of the ethmoid cartilage anteriorly.

Axial skeleton

The pattern of development of the axial skeleton can be inferred from the few larval specimens at hand with the ossification of the autocentra, the formation of the neural and haemal arches, and their spines. The first center of ossification of vertebrae (autocentra, dorsal, and ventral arcualia) is behind the head, with an antero-posterior direction of development (7.89 and 9.77 mm SL). A second center of ossification begins at the other end of the axial skeleton, with a postero-anterior direction of development (11.14 mm SL), with all vertebrae partially ossified by 13.82 mm SL (Fig. 7D). The development of the neural and haemal arches appears to be bi-directional, with fully developed arches and spines in the middle of the body and less developed cartilaginous spines posteriorly and anteriorly. Hence, the bi-directional ossification of the vertebrae (autocentra, dorsal, and ventral arcualia) is from ends to middle, but the neural and haemal spines are bi-directional from middle to ends.

Fins and girdles

The pectoral girdle bones missing dorsally, the posttemporal reduced to a flattened bone, and the extended length of the cleithrum and postcleithum, could be explained by the dorsal shift of the pectoral fin above the midline and the greater body depth at this point, as a functional response to the high energy environment of the surf zone (Saeed et al., 1994). The ventral extension of the cleithrum and postcleithrum bones provide the necessary support for the tear-drop body shape (Fig. 1) and protection of the slim peritoneal cavity. These extended bones have a further flaring of their ventral ends to form sharper and stronger ventral keels together with the pelvic girdle (Fig. 11A). These could all be functional modifications shared with *Iso* species for this surf zone environment or products of a common ancestor, depending on the phylogenetic relationships these groups share. This appealing functional explanation, however, still needs to be tested experimentally to determine whether the dorsal position of the pectoral fin, the tear-drop shape of the body, and the ventral keel have in fact any biomechanical advantage in turbulent waters.

A generalized condition in atherinomorphs is a pectoral-fin spur, a bony spur or nodule fused to the proximal end of the first ray as if it were a reduced pectoral fin spine (Dyer, 1997:35). No evidence is observed in the larval stages of a reduced or fused pectoral-fin spine. The first pectoral fin ray in *Notocheirus* has instead an enlarged medial hemitrichium proximally which is extended laterally and articulates with the posterior rim of the scapula (Fig. 8A).

The pelvic-fin girdles are sutured to each other by a strong pelvic symphysis in a *V*-shaped position. Each bone has a very thin layer of intervening musculature between it and the inner lining, and ventrally their midlines are aligned to form a sharp ventral keel (Fig. 9B). The medio-ventral (Saeed et al., 1994) or postero-ventral process (Saeed et al., 2006) in *Iso* species is a posterior extension of the ventral keel. The posterior process in *Notocheirus* however, is very different in that it is a short posterior extension of the pelvic symphysis (Fig. 9, B and C). The pelvic bones are strongly articulated by a percoid-like symphysis, very different from the flattened and overlapping median processes in other atherinomorph taxa (Dyer, 1997). *Iso* species have no median processes and the pelvic bones are connected along the extended postero-ventral midline (Saeed et al., 2006). Also, *Notocheirus* has 2 distal radials whereas *Iso* has none.

The dorsal and anal fin rays and their pterygiophores are all cartilaginous in the larval stages observed and are partly ossified only in the juvenile specimen, so ossification must occur between 16 and 31 mm SL. Cartilaginous pterygiophores with some non-ossified fin rays are present in the anal (20) and dorsal (13) fins at 7.89 mm SL. More pterygiophores are added anteriorly and posteriorly in larger larval specimens. Richter and Moritz (2017) corroborated that for Atherinomorphae the ossification development pattern of the median fins and their supports is bi-directional, that is, ossification of pterygiophores and lepidotrichia begins in the middle of the fin

and progresses anteriorly and posteriorly until fully ossified. The novel atheriniform development of the first dorsal fin, described by Richter and Moritz (2017), cannot be addressed in *Notocheirus* by it lacking this fin.

A leading flexible fin spine, followed by unbranched and branched segmented rays connected to cartilaginous distal radials, is the widespread condition in atheriniforms for the anal and second dorsal fins (Dyer and Chernoff, 1996; Richter and Moritz, 2017). This is also the case in *Notocheirus*, except that the procurrent ray is not fused into a single bony piece in the juvenile specimen, but remains as 2 unsegmented and unbranched hemilepidotrichs connected to the first proximal radial of the anal fin or to the first distal radial of the dorsal fin (Figs. 10 and 11C; procurrent rays sensu Arratia, 2008). Whether the procurrent rays remain as such or fuse into a single flexible spine as in other atheriniforms needs to be corroborated in adult specimens.

The posterior-most proximal radial of both median fins in *Notocheirus* was described by Dyer and Chernoff (1996:40) as having only one fin ray in *Notocheirus* instead of 2 fin rays articulated with a single distal radial. This is corrected herein for *Notocheirus* to have 2 small fin rays articulated with an elongated distal radial in both median fins (Fig. 10).

Caudal fin

The epural is lacking in the caudal fin of juveniles and adults, which is regarded as a diagnostic feature for this monotypic genus. This study has shown a larval epural to be present in specimens 9.77–15.42 mm SL (Fig. 7, B–E); still connected to the posterior neural arch of preural centrum 2 in specimens 7.89, 11.14, and 15.42 mm SL (Fig. 7, C and E); present but not connected to a posterior neural arch (Fig. 7, B and D); and later reabsorbed or fused to the neural spine of preural centrum 2 in specimens 16.21 and 31.16 mm SL (Fig. 7A) and adult stages (Saeed et al., 2006). Hence, the absence of an epural in adults cannot be considered a case of paedomorphism as suggested by Saeed et al. (2006). This condition needs to be reassessed for phylogenetic studies because though it is present in the larval stages of *Notocheirus* and fused in juveniles and adults, a single epural is nevertheless present in species of *Iso*, *Notocheirus*, and *Dentatherina* and hence, a derived feature when compared to the plesiomorphic condition of 2 epurals (Saeed et al., 1994, 2006).

Conclusions

The presence of odontodes on dermal bones of the head and spinoid scales on the head and body of *Notocheirus* has been mentioned since the description of *N. hubbsi* (Clark, 1937; Rosen, 1964; Saeed et al., 1994; Dyer and Chernoff, 1996; Saeed et al., 2006). These odontodes and spinoid scales are absent in larval stages, and are present only in juveniles and adults, but not in all specimens. A novel feature is the crown of spines on the snout, a ring-like formation of odontodes not connected to any underlying bone (Figs. 2, 3, A and B, and 11A). This structure is a unique dermal formation not seen elsewhere in Atherinomorphae. More specimens are needed to address the question of presence or absence of these odontode formations in juveniles and adults. The supraorbital sensory canal of *Notocheirus* has a derived pattern of pore openings on the frontal bone in which pore 5 opens medially, as do species of Atherinopsinae, *Iso*, and Melanotaenidae (Dyer, 1997). This morphological feature fits partially with the genomic-based phylogenetic hypothesis of atheriniform relationships (Bloom et al., 2012) in that *Notocheirus* is a member of Atherinopsidae, but conflicts with Menidiinae as its sister group and *Iso* as sister group to Atherinidae (Campanella et al., 2015). Another character that is novel to this study is the presence of a single epural in the caudal skeleton of larval stages in *Notocheirus* (Fig. 7, B–E). Previous studies have claimed *Notocheirus* lacking an epural bone, *Iso* and *Dentatherina* with one epural, and most atheriniforms sharing 2 epurals (Rosen, 1964; Saeed et al., 1994). This study shows the presence of a larval epural bone that is later fused to the neural spine of preural centrum 2 or is reabsorbed at the juvenile stage (Fig. 7A). The presence of one epural bone shared by *Notocheirus* and *Iso* adds another character to the 6 diagnostic features listed by Dyer and Chernoff (1996) in support of a sister group relationship between these 2 taxa instead of *Iso* placed in its own family, as sister group to Atherinidae (Campanella et al., 2015).

This species is notable also for the bones it is lacking or that are greatly reduced in the ethmoid region, branchial basket, posterior region of neurocranium and paired fins. These regions have all been affected by the acquisition of its tear-drop body shape which involves a shortening of the snout and jaws and an increase in body depth in the postcranial region. An apparent consequence of this tear-drop body shape is the curvature of the parasphenoid and the novel feature of it tunneled through the interorbital cartilage to be attached to the ventral surface of the ethmoid cartilage. In addition, the paired fins are also modified in that the pectoral fins are displaced dorsally above the horizontal septum and the girdle is extended ventrally to form a ventral keel (Fig. 11A) together with the pelvic girdles. These are flattened and placed in a *V*-shaped disposition with a strong articulation between them and connected by ligament to a rib (Fig. 9). The often-cited adaptation of this tear-drop body form to a surf environment has not been yet experimentally tested.

Acknowledgments

We appreciate Professor Donald Brown's assistance in taking the pictures of the cleared and stained individuals. We wish to thank Sergio Carrasco for loaning us the specimen of Figure 1, and especially for the many comments, suggestions, and corrections made by Gloria Arratia and the anonymous reviewers that significantly improved the comparative anatomy of the developmental process. This research was funded by the Comisión Nacional de Ciencia y Tecnología (CONICYT, Chile), FONDECYT 1150296 grant to MFL.

Literature cited

Arratia, G.
2008. Actinopterygian postcranial skeleton with special reference to the diversity of fin ray elements, and the problem of identifying homologies. *In* Mesozoic fishes 4: homology and phylogeny (G. Arratia, H.-P. Schultze, M. V. H. Wilson, eds.), p. 49–101. Verlag Dr. Friedrich Pfeil, München, Germany.

Arratia, G., H.-P. Schultze, and J. Casciotta.
2001. Vertebral column and associated elements in dipnoans and comparison with other fishes: development and homology. J. Morphol. 250:101–172. https://doi.org/10.1002/jmor.1062

Betancur-R, R., E. O. Wiley, G. Arratia, A. Acero, N. Bailly, M. Miya, G. Lecointre, and G. Ortí.
2017. Phylogenetic classification of bony fishes. BMC Evol. Biol. 17:162. https://doi.org/10.1186/s12862-017-0958-3

Bloom, D. D., P. J. Unmack, A. E. Gosztonyi, K. R. Piller, and N. R. Lovejoy.
2012. It's a family matter: molecular phylogenetics of Atheriniformes and the polyphyly of the surf silversides (Family: Notocheiridae). Mol. Phylogenet. Evol. 62:1025–1030. https://doi.org/10.1016/j.ympev.2011.12.006

Bräger, Z., and T. Moritz.
2016. A scale atlas for common Mediterranean teleost fishes. Vertebr. Zool. 66:275–386. https://doi.org/10.3897/vz.66.e31566

Campanella, D., L. C. Hughes, P. J. Unmack, D. D. Bloom, K. R. Piller, and G. Ortí.
2015. Multi-locus fossil-calibrated phylogeny of Atheriniformes (Teleostei, Ovalentaria). Mol. Phylogenet. Evol. 86:8–23. https://doi.org/10.1016/j.ympev.2015.03.001

Carrasco, S. A., L. Vandecasteele, M. M. Rivadeneira, M. Fernández, and A. Pérez-Matus.
2017. Spatial and short-term variability of larval, post-larval and macrobenthic assemblages associated with subtidal kelp forest ecosystems in Central Chile. Mar. Biol. Res. 13:1041–1058. https://doi.org/10.1080/17451000.2017.1322704

Clark, H. W.
1937. New fishes from the Templeton Crocker Expedition of 1934–35. Copeia 1937:88–91. https://doi.org/10.2307/1436949

Díaz-Astudillo, M., M. F. Landaeta, V. Bernal-Durán, M. I. Castillo, M. Alvarado-Niño, and D. Alarcón.
2019. The influence of regional and local oceanography in early stages of marine fishes from temperate rocky reefs. Mar. Biol. 166:42. https://doi.org/10.1007/s00227-019-3489-1

Dingerkus, G., and L. D. Uhler.
1977. Enzyme clearing of alcian blue stained whole small vertebrates for demonstration of cartilage. Stain Technol. 52:229–232. https://doi.org/10.3109/10520297709116780

Dyer, B. S.
1997. Phylogenetic revision of Atherinopsinae (Teleostei, Atherinopsidae), with comments on the systematics of the South American freshwater fish genus *Basilichthys* Girard. Misc. Publ., Mus. Zool., Univ. Mich. 185, 64 p.
2000. Systematic review of the silverside fishes of Chile (Teleostei, Atheriniformes). Est. Oceanol. 19:99–127. [In Spanish.]
2006. Systematic revision of the South American silversides (Teleostei: Atheriniformes). Biocell 30(Suppl.S):69–88.

Dyer, B. S., and B. Chernoff.
1996. Phylogenetic relationships among atheriniform fishes (Teleostei: Atherinomorpha). Zool. J. Linn. Soc. 117:1–69. https://doi.org/10.1111/j.1096-3642.1996.tb02148.x

Fricke, R., W. N. Eschmeyer, and R. Van der Laan (eds.).
2024. Eschmeyer's Catalog of Fishes: genera, species, references. [Available from https://www.calacademy.org/scientists/projects/eschmeyers-catalog-of-fishes, accessed June 2024.]

Gosline, W. A.
1949. The sensory canals of the head in some cyprinodont fishes, with particular reference to the genus *Fundulus*. Occas. Pap. Mus. Zool. Univ. Mich. 519, 17 p.

Gosztonyi, A. E.
1972. *Notocheirus hubbsi* Clark 1937 (Pisces, Isonidae), adición a la fauna Argentina de peces marinos. Physis 31(83):579–583.

Mancini, M., F. Grosman, B. Dyer, G. García, O. Del Ponti, P. Sanzano, and V. Salinas.
2016. Pejerreyes del sur de América: aportes al estado de conocimiento con especial referencia a *Odontesthes bonariensis*, 280 p. UniRío Editora, Río Cuarto, Argentina.

Nelson, J. S., T. C. Grande, and M. V. H. Wilson.
2016. Fishes of the world, 5th ed., 752 p. Wiley, New York.

Richter, P., and T. Moritz.
2017. Lessons from the first dorsal fin in atheriniforms—a new mode of dorsal fin development and its phylogenetic implications. J. Morphol. 278:848–864. https://doi.org/10.1002/jmor.20679

Roberts, C. D.
1993. Comparative morphology of spined scales and their phylogenetic significance in the Teleostei. Bull. Mar. Sci. 52:60–113.

Rosen, D. E.
1964. The relationships and taxonomic position of the halfbeaks, killifishes, silversides, and their relatives. Bull. Am. Mus. Nat. Hist. 127:217–268.

Saeed, B., W. Ivantsoff, and L. E. L. M. Crowley.
1994. Systematic relationships of atheriniform families within Division I of the Series Atherinomorpha (Acanthopterygii) with relevant historical perspectives. J. Ichthyol. 34:27–72.

Saeed, B., W. Ivantsoff, and A. Aarn.
2006. Descriptive anatomy of *Iso rhothophilus* (Ogilby), with

a phylogenetic analysis of *Iso* and a redefinition of Isonidae (Atheriniformes). Aqua 11:25–43.

Said, B. M.
1983. Revision of the fish genus *Iso*. M.S. thesis,177 p. Macquarie Univ., New South Wales, Australia. [Available from Macquarie University Library, 16 Macquarie Walk, Macquarie Park, NSW 2109, Australia.]

Schultze, H.-P.
2008. Nomenclature and homologization of cranial bones in actinopterygians. *In* Mesozoic fishes 4: homology and phylogeny (G. Arratia, H.-P. Schultze, and M. V. H. Wilson, eds.), p. 23–48. Verlag Dr. Friedrich Pfeil, München, Germany.

Schultze, H.-P., and G. Arratia.
1989. The composition of the caudal skeleton of teleosts (Actinopterygil [*sic*]: Osteichthyes). Zool. J. Linn. Soc. 97:189–231. https://doi.org/10.1111/j.1096-3642.1989.tb00547.x

Sire, J.-Y., and F. Allizard.
2001. A fourth teleost lineage possessing extra-oral teeth: the genus *Atherion* (Teleostei; Atheriniformes). Eur. J. Morphol. 39:295–305. https://doi.org/10.1076/ejom.39.5.0295

Thieme, P., P. Warth, and T. Moritz.
2021. Development of the caudal-fin skeleton reveals multiple convergent fusions within Atherinomorpha. Front. Zool. 18:20. https://doi.org/10.1186/s12983-021-00408-x

Zavala-Muñoz, F., M. F. Landaeta, V. Bernal-Durán, C. A. Bustos, and B. S. Dyer.
2021. Abundance of early life stages of the surf silverside *Notocheirus hubbsi* (Teleostei, Atheriniformes) in the coastal nearshore of central Chile. Rev. Biol. Mar. Oceanogr. 56:74–77. https://doi.org/10.22370/rbmo.2021.56.1.2800

Published online 10 July 2024.

Cite as: Dyer, B. S., F. Zavala-Muñoz, V. Bernal-Durán, and M. F. Landaeta. 2024. Osteological development of the surf silverside (*Notocheirus hubbsi*) (Teleostei: Atheriniformes: Notocheiridae). *In* Early Life History and Biology of Marine Fishes: Research inspired by the work of H Geoffrey Moser (J. M. Leis, W. Watson, B. C. Mundy, and P. Konstantinidis, guest eds.), p. 57–80. NOAA Professional Paper NMFS 24. https://doi.org/10.7755/PP.24.5